American Journal of Pathology, Vol. 167, No. 1, July 2005

Neurobiology

Developmental Abnormalities of Neuronal Structure and Function in Prenatal Mice Lacking the Prader-Willi Syndrome Gene Necdin

Silvia Pagliardini,* Jun Ren,* Rachel Wevrick,† and John J. Greer*

From the Department of Physiology, Centre for Neuroscience, and the Department of Medical Genetics,† University of Alberta, Edmonton, Alberta, Canada*

Necdin (*Ndn*) is one of a cluster of genes deleted in the neurodevelopmental disorder Prader-Willi syndrome (PWS). *Ndn*^{tm2Stw} mutant mice die shortly after birth because of abnormal respiratory rhythmogenesis generated by a key medullary nucleus, the pre-Bötzinger complex (preBötC). Here, we address two fundamental issues relevant to its pathogenesis. First, we performed a detailed anatomical study of the developing medulla to determine whether there were defects within the preBötC or synaptic inputs that regulate respiratory rhythmogenesis. Second, *in vitro* studies determined if the unstable respiratory rhythm in *Ndn*^{tm2Stw} mice could be normalized by neuromodulators. Anatomical defects in *Ndn*^{tm2Stw} mice included defasciculation and irregular projections of axonal tracts, aberrant neuronal migration, and a major defect in the cytoarchitecture of the cuneate/gracile nuclei, including dystrophic axons. Exogenous application of neuromodulators alleviated the long periods of slow respiratory rhythms and apnea, but some instability of rhythmogenesis persisted. We conclude that deficiencies in the neuromodulatory drive necessary for preBötC function contribute to respiratory dysfunction of *Ndn*^{tm2Stw} mice. These abnormalities are part of a more widespread deficit in neuronal migration and the extension, arborization, and fasciculation of axons during early stages of central nervous system development that may account for respiratory, sensory, motor, and behavioral problems associated with PWS. *(Am J Pathol 2005, 167:175–191)*

Prader-Willi syndrome (PWS) is a contiguous gene deletion syndrome that occurs at a frequency of ~1:15,000 births. Symptoms are variable and include transient infantile hypotonia, failure to thrive, hyperphagia leading to severe obesity, somatosensory deficits, behavioral problems, and mild to moderate mental retardation.[1,2] Further, PWS is associated with respiratory instability in the newborn period that is manifest as apneas and blunted chemosensitivity.[2–10]

The genetic defect in PWS patients (paternal deletions, maternal disomy, or imprinting mutations) results in the inactivation of paternally expressed genes on chromosome 15q11-q13.[11] To gain a better understanding of the function of individual genes within the loci, mouse models with a deficiency of paternal gene expression in the orthologous 7C chromosomal region have been generated. This has included mice deficient in necdin, one of four known protein-coding genes that are deficient in PWS.[12–14] Three necdin-deficient mouse strains were independently generated with two of the strains demonstrating neonatal lethality of variable penetrance.[15–17] Death of *Ndn*-null mouse pups occurred during the immediate neonatal period because of severe hypoventilation.[15,16] The source of the respiratory dysfunction was traced to abnormal respiratory neuronal activity within the pre-Bötzinger complex (preBötC), a key medullary structure responsible for respiratory rhythmogenesis.[18] Here, we extend on that study by addressing two fundamental questions. First, are there anatomical abnormalities within neuronal structures of the developing medulla and spinal cord in *Ndn*^{tm2Stw} mice that could account for respiratory and other central nervous system (CNS) related dysfunction? Second, is the abnormal breathing pattern in *Ndn*^{tm2Stw} mice due to intrinsic defects within preBötC or can it be accounted for by abnormalities of modulatory

Supported by the Canadian Institutes of Health (CIHR) (to J.R. and S.P.) and the Alberta Heritage Foundation for Medical Research (studentships to J.R. and S.P.) J.J.G. is an Alberta Heritage Foundation for Medical research scientist; and R.W. is an Alberta Heritage Foundation for Medical Research senior scholar.

Accepted for publication March 29, 2005.

Address reprint requests to John J. Greer, 513 HMRC Bldg., University of Alberta, Edmonton, AB, T6G 2S2 Canada. E-mail: john.greer@ualberta.ca.

Table 1. Antibodies

Antigen	Dilution	Antibody	Source	References
Neurofilament-2H3 (NF)	1:2000	Monoclonal (mouse IgG)	Dev. Studies Hybridoma Bank, Iowa	20
Neurofilament 150 kd	1:2000	Polyclonal (rabbit)	Chemicon, Temecula, CA	21, 22
Growth-associated protein 43 (GAP43)	1:2000	Monoclonal (mouse IgG)	Sigma, St. Louis, MO	23
Vimentin 40E-C (VIM)	1:200	Monoclonal (mouse IgM)	Dev. Studies Hybridoma Bank	24
Transiently expressed axonal glycoprotein clone 4D7 (TAG1)	1:200	Monoclonal (mouse IgM)	Dev. Studies Hybridoma Bank	20, 25
Substance P receptor (NK1R)	1:1000	Polyclonal (rabbit)	Advanced Targeting Systems, San Diego, CA	26, 27
Cell adhesion molecule L1 (L1)	1:200	Monoclonal (rat)	Chemicon	20
Choline acetyl transferase (ChAT)	1:300	Polyclonal (goat)	Chemicon	28
Substance P (SubP)	1:500	Monoclonal (rat)	Chemicon	29
Serotonin (5HT)	1:1000	Goat	Chemicon	30
Somatostatin (SST)	1:1000	Polyclonal (rabbit)	Immunostar, Hudson, WI	31
Tyrosine hydroxylase (TH)	1:2000	Polyclonal (rabbit)	Chemicon	22

neuronal inputs that regulate respiratory rhythmogenesis? These data demonstrate abnormalities in respiratory related nuclei and further widespread developmental anomalies that may account for other sensory, motor, and behavioral deficits associated with PWS.

Materials and Methods

Mouse Breeding and Genotyping

Procedures for animal care were approved by the Animal Welfare Committee at the University of Alberta. *Ndn*^{tm2Stw} mice were bred through the maternal line with C57BL/6J male mice. Male offspring carrying a maternally inherited *Ndn*^{tm2Stw} are phenotypically normal and were bred to C57BL/6J females to produce experimental embryos and offspring. In these litters, one-half of the mice are wild type and one-half carry a paternally inherited necdin deficiency and are functionally null. The timing of pregnancies was determined from the appearance of sperm plugs in the breeding cages, and the embryonic age of mice was confirmed by measuring crown-rump length.[19] Identification of mutant offspring was performed by histochemical detection of β-galactosidase activity and by polymerase chain reaction genotyping of snap-frozen tissue with *lacZ* oligonucleotide primers (LACZ1942F, 5′GTGTCGTTGCTGCATAAACC; and LACZ2406R, 5′TCGTCTGCTCATCCATGACC).

Animal Handling for Anatomical Studies

Fetal mice were delivered from timed pregnant animals anesthetized with halothane (1.5% delivered in 95% O_2 and 5% CO_2) and transcardially perfused with 4% paraformaldehyde or 4% paraformaldehyde-2.5% glutaraldehyde in phosphate buffer at pH 7.2. Brainstems, spinal cords, and diaphragms were dissected out and postfixed in the same fixative solution; tissue was embedded in agar and cut on a vibratome (VT1000S; Leica, Germany) for single- and double-labeling immunohistochemistry.

Immunohistochemistry

To examine the detailed neuroanatomy of *Ndn*^{tm2Stw} mice, we analyzed brainstem and spinal cord distribution of several anatomical and neuronal markers (see Table 1 for antibodies used and their references,[20–31]) from embryonic day (E)10 to E18. Mutant and wild-type mice within the same litter were processed together for comparisons. Transverse and sagittal sections (50 μm) were serially collected in phosphate-buffered saline (PBS) and immunoreacted according to the following protocol. Free-floating sections were incubated with 1.0% bovine serum albumin (BSA; Sigma Chemical Co., St. Louis, MO) and 0.2 to 0.3% Triton X-100 in PBS for 60 minutes to reduce nonspecific staining and to increase antibody penetration. Sections were incubated overnight with primary antibodies diluted in PBS containing 0.1% BSA and 0.2 to 0.3% Triton X-100. The following day, sections were washed in PBS and incubated with specific secondary antibodies diluted in PBS and 0.1% BSA for 2 hours (biotin-, Cy3-, Cy5- or Cy2-conjugated donkey anti-rabbit, donkey anti-goat, donkey anti-rat, donkey anti-mouse IgG or donkey anti-mouse IgM; 1:200; all purchased from Jackson ImmunoResearch, West Grove, PA). Sections were further washed in PBS and those immunoreacted with fluorescent-conjugated secondary antibodies were mounted and coverslipped with Fluorsave mounting medium (Calbiochem, La Jolla, CA). In some experiments, sections were counterstained with Hoechst 33342 (Molecular Probes, Eugene, OR). When biotin-conjugated secondary antibodies were used, sections were labeled using a peroxidase method. After washes in PBS, sections were incubated with standard peroxidase-conjugated ABC kit (1:100; Vector Laboratories, Burlingame, CA) for a further 2 hours. The reaction was detected with 0.08% diaminobenzidine (DAB) and 0.007% H_2O_2 in Tris-HCl buffer. Adjacent sections were counterstained with thionine (1%) to visualize tissue cytoarchitecture. DAB-immunostained sections were analyzed with an Olympus BX40 microscope and images were taken with a SPOT-digital Microscope camera (Carsen, Markham, ON) connected to a computer running Image-Pro-Plus software

(Media Cybernetics Inc., Silver Spring, MD). Acquired images were exported in TIFF format, and brightness and contrast adjusted in Adobe Photoshop 7.0.

Confocal Imaging

Immunostained sections were examined and processed using a Zeiss100M microscope, LSM510 NLO laser, and LSM510 software. For Cy2, Cy3, and Cy5 fluorescence, excitation was set to 488, 543, and 633 nm and emissions were collected with 505-, 560-, and 630-nm long-pass filters, respectively. For Hoechst 33342 fluorescence, a two-photon laser was used with the excitation set at 780 nm and emissions collected using a 390- to 465-nm band pass filter. Thin sections and multiple sectioning acquisitions along the z-plane were performed to obtain a suitable signal through the depth of the section. Acquired images were then exported in JPEG format, and brightness and contrast adjusted in Photoshop 7.0.

Volumetric Measurements and Cell Counts

Measurements of areas of motoneuronal pools, dorsal fasciculus, and anterolateral funiculus were obtained from confocal acquired images of serial sections of brainstem and spinal cord (E11 to E18). Surface area of vagus, ambiguus, and hypoglossal nuclei was measured bilaterally for each section and an average area was calculated for each animal by means of LSM510 software. For motoneuronal pools of E18 brainstems and cervical spinal cords, a cell count was also performed and an average cell density determined for each pool. Varicosities immunolabeled for serotonin, substance P, and tyrosine hydroxylase and the dystrophic structures were analyzed by means of LSM510 software and an average area of the varicosities determined. Paired *t*-tests comparing *Ndn*^{tm2Stw} mice to wild-type littermates were applied to determine statistical significance at $P < 0.05$.

Electron Microscopy

For electron microscopy immunohistochemistry, 50-μm free-floating sections were processed with pre-embedding immunoperoxidase. Sections were permeabilized by freeze-thawing at −80°C,[32] rinsed in PBS, treated with 1% H_2O_2 in PBS, and incubated with 1.0% BSA to mask nonspecific absorption sites. Sections were incubated with the primary anti-neurofilament (NF) antibody, biotinylated secondary antibody (DAM), and ABC complex as specified above. Peroxidase staining was obtained by incubating the sections in 0.048% DAB, 0.024% $CoCl_2$, 0.019% NAS, and 0.003% H_2O_2 in 0.1 mol/L phosphate buffer. All sections were extensively washed, osmicated in 1% OsO_4 in 0.1 mol/L phosphate buffer for 20 minutes, dehydrated in ethanol, and flat-embedded in TAAB812 Epon. Thin sections were counterstained with uranyl acetate and lead citrate and examined using a Philips 410 transmission electron microscope.

Brain Stem-Spinal Cord and Medullary Slice Preparations

Fetal mice (E18) were decerebrated and the brain stem-spinal cord with or without the ribcage and diaphragm muscle attached was dissected following procedures similar to those established previously.[33,34] The neuraxis was continuously perfused at 27 ± 1°C (perfusion rate, 5 ml/minute; chamber volume, 1.5 ml) with mock cerebral spinal fluid that contained (mmol/L): 128 NaCl, 3.0 KCl, 1.5 $CaCl_2$, 1.0 $MgSO_4$, 24 $NaHCO_3$, 0.5 NaH_2PO_4, and 30 D-glucose equilibrated with 95% O_2-5% CO_2. Details of the medullary slice preparation have been previously described.[35] Briefly, the brain stem was sectioned serially using a Leica vibratome in the transverse plane starting from the rostral medulla to within ~150 μm of the rostral boundary of the preBötC, as judged by the appearance of the inferior olive. A single transverse slice containing the preBötC and more caudal reticular formation regions was then cut (~500 μm thick), transferred to a recording chamber, and pinned down onto a Sylgard elastomer.

Recording and Analysis

Recordings of hypoglossal (XII) cranial nerve roots, cervical (C4) ventral roots, and diaphragm EMG were made with suction electrodes. Further, suction electrodes were placed into XII nuclei and the preBötC to record extracellular neuronal population discharge from medullary slice preparations. Signals were amplified, rectified, low-passed filtered, and recorded on computer using analog-digital converter (Digidata 1200; Axon Instruments) and data acquisition software (Axoscope, Axon Instruments).

Results

Results were obtained from *Ndn*^{tm2Stw} and wild-type mice to elucidate the 1) cytoarchitectural features of the medulla and spinal cord at various embryonic developmental stages, 2) innervation pattern of the diaphragm muscle, and 3) modulation of respiratory neuronal discharge of *in vitro* preparations in response to exogenous application of neurotransmitter receptor agonists.

General Cytoarchitectural Features in the Medulla of Ndn^{tm2Stw} *Mice*

Ndn^{tm2Stw} mice weighed ~17% less than wild-type mice on average (0.94 ± 0.04 g, $n = 12$ versus 1.13 ± 0.05 g, $n = 11$). As shown in Figure 1, the general appearance of the cytoarchitecture of *Ndn*^{tm2Stw} mice at different levels of the medulla is similar to wild-type mice from the same litters at E18. No significant differences in the location of major nuclei were observed. However, on closer examination, it was apparent that clearly identifiable motoneuronal nuclei in the brainstem including the nucleus ambiguus (NA), dorsal motor nucleus of the vagus (X), and hypoglossal nucleus (XII) were reduced in size. Statistical

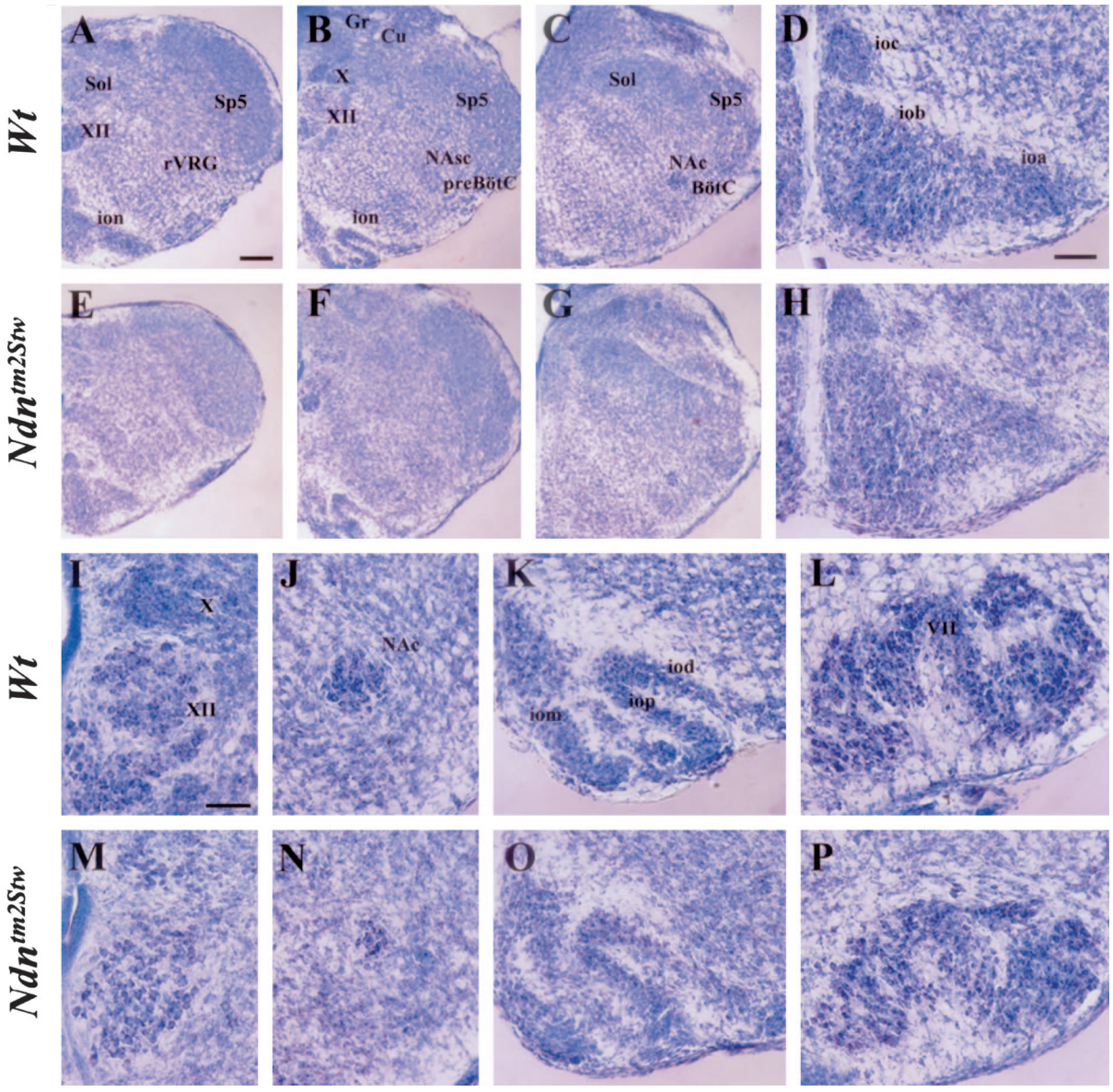

Figure 1. Cytoarchitectural abnormalities in the medulla of *Ndn*^{tm2Stw} mice. Transverse sections of the medulla stained with thionine from wild-type (**A–D** and **I–L**) and *Ndn*^{tm2Stw} mice (**E–H** and **M–P**) at the level of the rostral ventral respiratory group (rVRG; **A**, **D**, **E**, **H**, **I**, **M**), the pre-Bötzinger complex (preBötC; **B**, **F**, **J**, **K**, **N**, **O**), the Bötzinger complex (BötC; **C–G**), and the facial nucleus (VII; **L**, **P**). **D**, **H:** There are no major defects in the three subnuclei (**A–C**) of the caudal region of the inferior olive (ioa, iob, ioc). Hypoglossal nucleus (XII; **I**, **M**), dorsal nucleus of the vagus nerve (X), compact and semicompact formations of the nucleus ambiguus (NAc, NAsc; **J**, **N**) are smaller in *Ndn*^{tm2Stw} mice in comparison to wild-type mice. **K**, **O:** Medial, principal, and dorsal nuclei of the inferior olive (iom, iop, iod) are less finely organized in *Ndn*^{tm2Stw} mice in comparison to wild-type mice. **L**, **P:** Facial nucleus is similar in wild-type and *Ndn*^{tm2Stw} mice. Cu, cuneate nucleus; Gr, gracile nucleus; Sol, solitary tract nucleus; Sp5, spinal trigeminal nucleus. Scale bars: 200 μm (**A–C**, **E–G**); 100 μm (**D**, **H–P**).

analysis of the volumetric extension of the nuclei determined that the size of the nuclei is significantly different at E18 between control and mutant animals ($n = 4$). Specifically, the average area of the hypoglossal, vagus, and ambiguus nuclei at E18 were reduced by 66 ± 6.6%, 20 ± 4.5%, and 32 ± 3.3%, respectively, in mutant versus wild-type mice. We did not note any statistical difference in cell density in any of the nuclei. Further, the nuclei were clearly smaller at ages E12 to E14, before the major period of neuronal cell death.[36,37] The medial, dorsal, and principal subnuclei of the inferior olive were present, but their general shape was less organized and delineated in all of the *Ndn*^{tm2Stw} mice examined relative to the wild type.

Immunostaining for NF in transverse sections of the medulla at E18 revealed further abnormalities in *Ndn*^{tm2Stw} mice (Figure 2). First, throughout the medulla, the reticular formation had an irregular pattern. Cross sections of rostrocaudally extending axonal bundles of both sensory and motor pathways (eg, medial lemniscus in Figure 2, D and G) were reduced in size. Further, the axonal tracts were not as tightly fasciculated and the characteristic latticework-like pattern present in wild-type mice was disorganized. Contralateral fibers running in

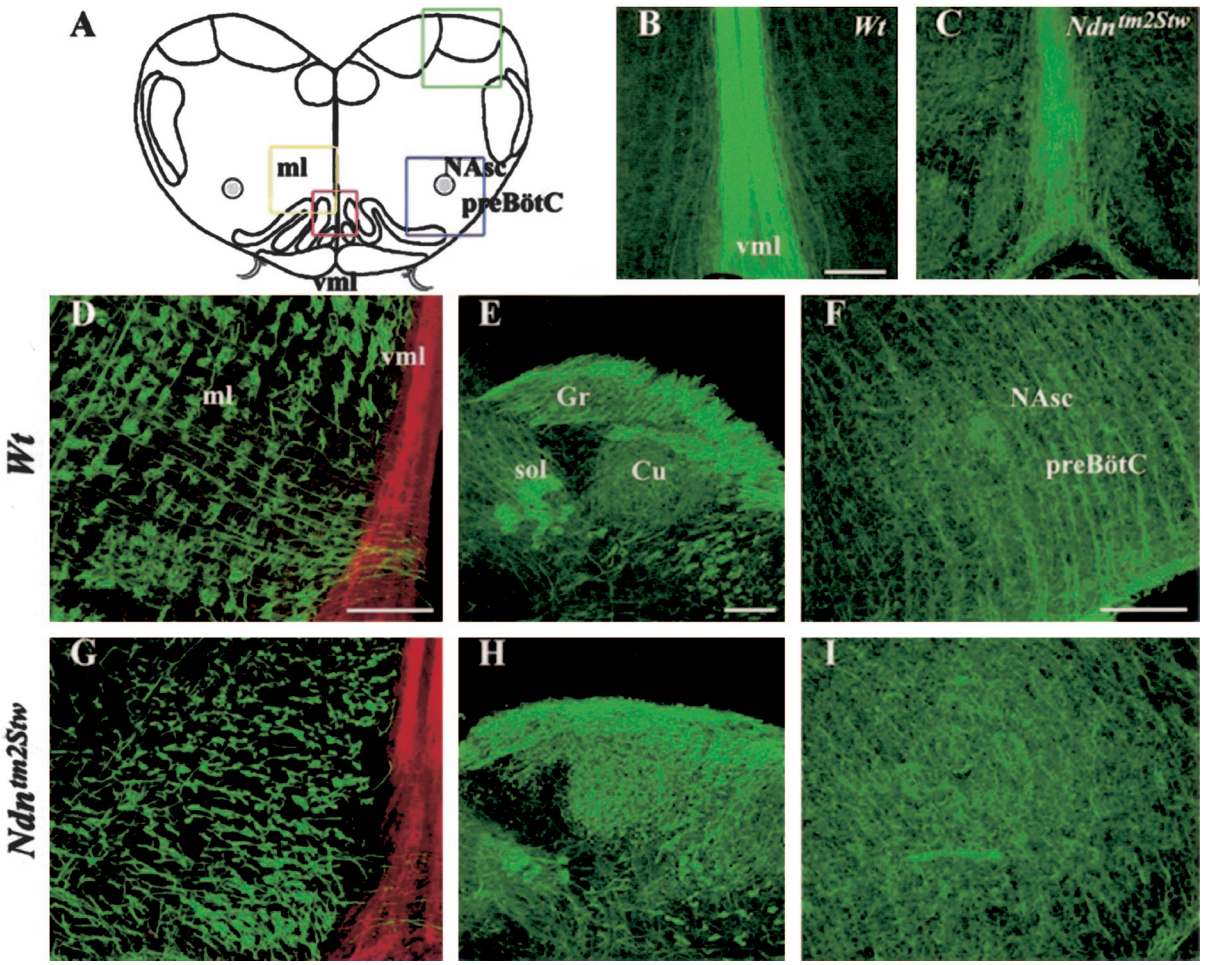

Figure 2. NK1R, NF, and vimentin expression in wild-type (**B**, **D–F**) and *Ndn*^{tm2Stw} mice (**C**, **G–I**) at E18. **A:** Schematic drawing of the medulla at the level of the preBötC. The **colored squares** delineate different areas of the medulla shown in the panels. Red, **B**, **C**; yellow, **D**, **G**; green, **E**, **H**; blue, **F**, **I**. **B** and **C:** Vimentin expression shows a clear disarrangement in the organization of the ventral midline (vml) in *Ndn*^{tm2Stw} in comparison to wild-type mice. **D** and **G:** NF (green) and NK1R (red) expression in the medial lemniscus (ml) lateral to vml. **G:** Note the reduced size and the defasciculation of axonal bundles through the ventral medulla in *Ndn*^{tm2Stw} mice. **E** and **H:** At the level of the gracile (Gr) and cuneate (Cu) nuclei and funiculi, NF labels dystrophic structures in *Ndn*^{tm2Stw} mice. **F** and **I:** Disarrangement of the radial glia in *Ndn*^{tm2Stw} mice is shown by vimentin immunolabeling in the ventrolateral medulla. NAsc, nucleus ambiguus, semicompact formation; preBötC, pre-Bötzinger complex; sol, solitary tract. Scale bars: 100 μm (**B–I**).

the medulla, internal arcuate fibers, and cervical nerve roots, while present and positioned correctly were reduced in size and number.

In the dorsal medulla, NF labeling showed a reduced size and an irregular distribution of fibers in the solitary tract (Figure 2, E and H). The most striking feature observed was at the level of the dorsal column where sensory fibers in the cuneate and gracile nuclei were swollen and enlarged. Similar staining was observed at the level of the external cuneate nuclei and, to a minor extent, in the spinal trigeminal nucleus and in the cerebellum (data not shown).

We also examined the anatomical organization of radial glia in the developing medulla via immunolabeling for vimentin.[38] We were particularly interested in determining whether the abnormal bundling of axonal tracts described above could be related to disruptions in the normal pattern of radial glia that provide the major scaffolding system for neurite extension in the developing CNS.[39] Although vimentin expression was evident in radial glia in *Ndn*^{tm2Stw} mice, the typically precisely organized pattern was misplaced and the neuronal extensions were intermingled with the radial glia in a highly disorganized manner throughout the medulla (Figure 2; B, C, F, and I). Along the midline, where fibers were compact and highly organized in a dorsoventral pattern in wild-type mice, the immunolabeling for both vimentin (Figure 2, B and C) and neurokinin 1 receptor (NK1R) (Figure 2, D and G) showed an irregular and less compact organization of the midline in *Ndn*^{tm2Stw} mice. Figure 2, F and I, further illustrate the abnormal organization of the radial glia in the ventrolateral medulla.

Organization of Neuronal Subpopulations within the Medulla of Ndn^{tm2Stw} *Mice*

The lethal hypoventilation present in *Ndn*^{tm2Stw} mice was shown previously to be due to abnormal neuronal activity within the preBötC, a major site of inspiratory rhythmogenesis within the medulla.[18] NK1R expression has been used as a marker for the preBötC in both adult and

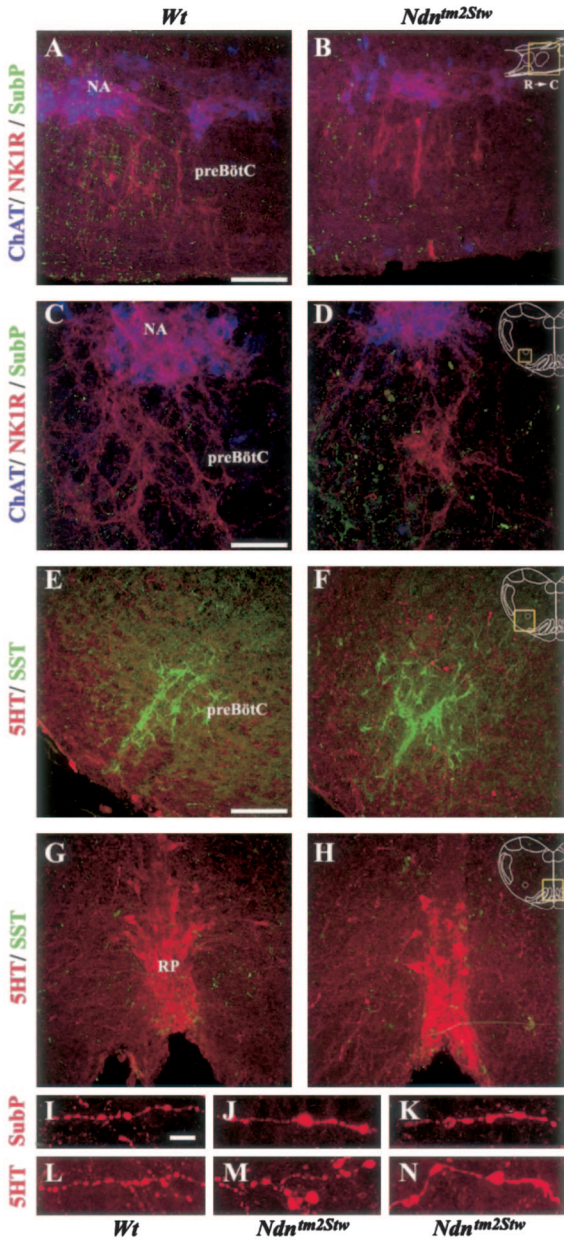

Figure 3. Expression of NK1R, ChAT, SubP, SST, and 5HT in the ventral medulla of wild-type (**A**, **C**, **E**, **G**, **I**, **L**) and *Ndn*^{tm2Stw} mice (**B**, **D**, **F**, **H**, **J**, **K**, **M**, **N**) at E18. In each set of figures (from **A** to **H**), a **yellow square** in the drawing indicates where the image was acquired. Sagittal (**A**, **B**) and transverse (**C**, **D**) sections immunoreacted for ChAT (blue), NK1R (red), and SubP (green) at the level of the preBötC show the reduced extension of the nucleus ambiguus (NA) in *Ndn*^{tm2Stw} mice. NK1R-immunopositive neurons in the preBötC area are present in both wild-type and *Ndn*^{tm2Stw} mice. Transverse sections immunoreacted for SST (green) and 5HT (red) at the level of the preBötC (**E**, **F**) and the raphe pallidus (RP;**G**, **H**) show no gross abnormalities in the SST-positive neurons at the level of the preBötC and in the 5HT-positive neurons of the caudal raphe nucleus. **I–N:** Details of abnormalities within SubP (**I–K**)- and 5HT (**L–N**)-immunopositive fibers in the preBötC region. Note the presence of enlarged varicosities in the irregularly oriented fibers. C, caudal; R, rostral. Scale bars: 200 μm (**A**, **B**); 50 μm (**C**, **D**); 100 μm (**E–H**); 10 μm (**I–N**).

perinatal animals.[40–45] Immunolabeling for NK1R in the ventrolateral medulla showed no obvious differences between wild-type and *Ndn*^{tm2Stw} mice (Figure 3; A to D, red). As shown in both sagittal and transverse sections, there was a reduction in size and extension of the NA (as already noted in thionine-stained sections in Figure 1), but the cluster of neurons ventral to the caudal end of the compact formation of the NA, the putative location of the preBötC, appeared normal.

A further immunohistochemical marker for preBötC neurons is somatostatin (SST,[31]). The SST expression was similar in both wild-type and *Ndn*^{tm2Stw} mice at the level of the preBötC (Figure 3, E and F). Thus, collectively, based on the current criteria for immunohistochemical classification of the preBötC area, there were no obvious anatomical abnormalities within this critical site for inspiratory rhythmogenesis in *Ndn*^{tm2Stw} mice.

We then turned our attention toward examining the organization of synaptic input from neuromodulatory systems that project to the preBötC and regulate inspiratory rhythmogenesis. Immunolabeling for substance P (SubP) within the preBötC area was clearly present in both sagittal (Figure 3, A and B, green) and transverse (Figure 3, C and D, green; and I to K, red) sections. SubP-positive fibers in the wild-type mice were fine and evenly distributed in the ventrolateral medulla (Figure 3; A, C, and I) with several synaptic boutons in the preBötC areas. In *Ndn*^{tm2Stw} mice, SubP-positive fibers were present, but they were enlarged and irregularly oriented within the ventrolateral medulla (Figure 3; B, D, J, and K).

Immunolabeling for serotonin (5HT) identified 5HT-positive neurons of the raphe nuclei (magnus, pallidus, and oralis) in the medulla and the pons. No major differences in the neuronal distribution or in the size of the different nuclei were observed (Figure 3, G and H), although 5HT-positive fibers within the ventrolateral medulla were also swollen and enlarged in mutants (Figure 3, E and F, red; and L to N). To better characterize the abnormalities in the distribution and morphology of SubP and 5HT fibers, we measured the areas of varicosities. The average area in control animals at E18 was 1.57 $\pm$ 0.9 μm^2 for 5HT fibers and 2.64 $\pm$ 0.15 μm^2 for SubP fibers. In *Ndn*^{tm2Stw} mice, the average area was significantly increased to 3.14 $\pm$ 0.14 μm^2 for 5HT fibers and 3.28 $\pm$ 0.32 μm^2 for SubP fibers.

Noradrenergic neurons located within the pons and medulla modulates the activity of the respiratory rhythm generating center.[46–49] We analyzed the distribution of immunoreactivity for tyrosine hydroxylase (TH), a marker for adrenergic and noradrenergic neurons.[50] The number of neurons and positive fibers in A2 and C2 groups (Figure 4, A and B), although slightly increased, were not significantly different in *Ndn*^{tm2Stw} and wild-type mice. However, the distribution and appearance of TH-positive neurons were clearly abnormal in other medullary regions. The abnormalities included aberrant TH-positive neurons located along the midline (C3 group), in the ventral noradrenergic bundle (Figure 4; C to F) and in the A1/C1 group in the ventrolateral medulla (Figure 4, G and H). Cell counts of TH-positive neurons demonstrated significant increases in A1/C1, ventral bundle, and C3/midline populations of 42 $\pm$ 9.5%, 133 $\pm$ 2.4%, and 230 $\pm$ 32.7%, respectively, in mutant versus wild-type animals (Figure 4K). Further, TH-positive fibers in several nuclei and within the ventral noradrenergic bundle were enlarged and dystrophic with some neurons having pro-

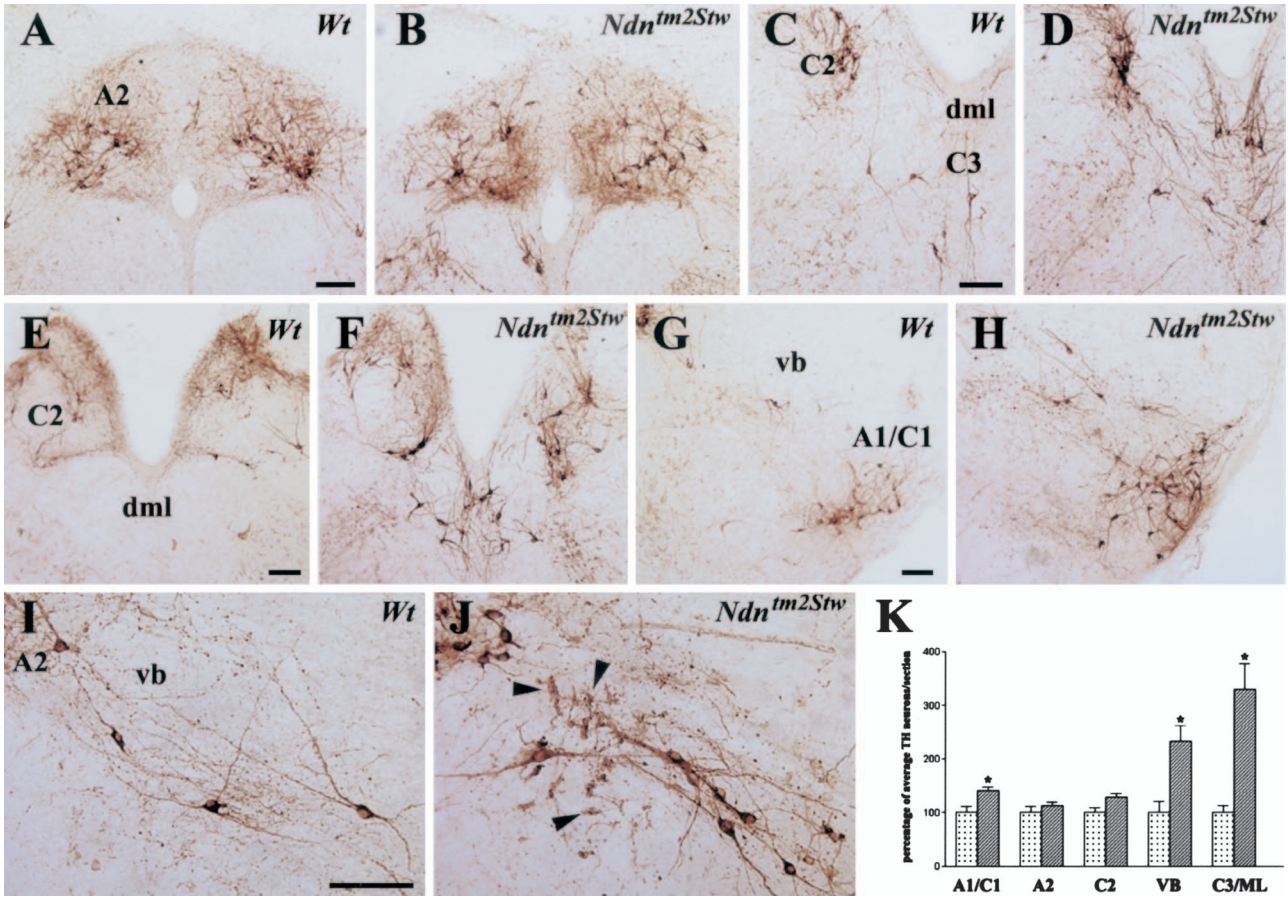

Figure 4. Expression of TH in the medulla of wild-type (**A**, **C**, **E**, **G**, **I**) and *Ndn*^{tm2Stw} mice (**B**, **D**, **F**, **H**, **J**). **A–F:** No major differences in cell number at the level of A2 noradrenergic and C2 adrenergic neurons are present between wild-type and *Ndn*^{tm2Stw} mice, although the TH-immunoreactive neuropil appears stronger in *Ndn*^{tm2Stw} mice. **C–F:** C3 adrenergic neurons in the dorsal midline of the medulla of *Ndn*^{tm2Stw} mice are more numerous that in wild-type mice. Note the presence of several TH-immunopositive neurons along the dorsal midline (dml; **D**, **F**). **C** and **D** are taken at more caudal level than **E** and **F**. **G** and **H:** The A1/C1 noradrenergic group also contains a larger number of TH-positive neurons in *Ndn*^{tm2Stw} mice in comparison to wild type. **I** and **J:** Ventral noradrenergic bundle in the reticular formation of the medulla. In *Ndn*^{tm2Stw} mice, the noradrenergic bundle contains a higher number of cell bodies and fibers. **K:** Relative percentage of adrenergic and noradrenergic neurons in the medulla of wild-type (**dotted bars**) and *Ndn*^{tm2Stw} mice (**striped bars**). **Asterisks** show differences that are statistically significant ($P < 0.05$). Scale bars, 100 μm (**A–J**).

cesses with a complex arborization (data not shown). The abnormal morphology of TH-positive fibers located in the ventral bundle was quantified by measuring their cross-sectional area in both control and mutant animals. The average size of TH-positive fibers in control mice was 2.09 ± 0.10 μm^2, whereas in the mutant mice the average size was significantly increased to 5.92 ± 0.41 μm^2. At more rostral levels, noradrenergic cell bodies in A5 group were more numerous and irregularly distributed and the fibers running along the ventral bundle and the contralateral fibers in the locus ceruleus were swollen, irregular, and dystrophic (data not shown).

Abnormalities within Medullary Dorsal Column Structures of Ndn^{tm2Stw} *Mice*

As shown in Figure 2, the most marked abnormalities were observed at the level of the cuneate and gracile nuclei. To further elucidate the nature of the abnormal staining detected within those regions, double-labeling experiments with antibodies against NF and the growth-associated protein 43 (GAP43) (Figure 5; A to C) were performed. There was no co-localization between NF and GAP43 within the spheroids, although very clear double labeling was present in adjacent fibers running in the fasciculi and through the brainstem, suggesting that dystrophic structures are not present in the still extending axons of the DRG neurons. These results suggest that dystrophic structures start appearing in the developing medulla after GAP43 is down-regulated and thus after axonal extension is completed.

To determine the timing of spheroid formation, we analyzed brainstem sections immunolabeled with NF during earlier stages of development (Figure 5; D to F). Spheroids were present as early as E15 and they were clearly distinguishable from the growth cones of sensory afferents (Figure 5E, arrows). In the putative area of the developing dorsal column, there were no NF-positive spheroids at earlier stages of development (Figure 5F, E13) and they progressively developed between E13 and E15. The nature of the spheroids was further investigated by means of specific neuroanatomical markers used to identify neuronal populations within the cuneate and gracile nuclei.[51,52] Immunolabeling of sections from the dorsal

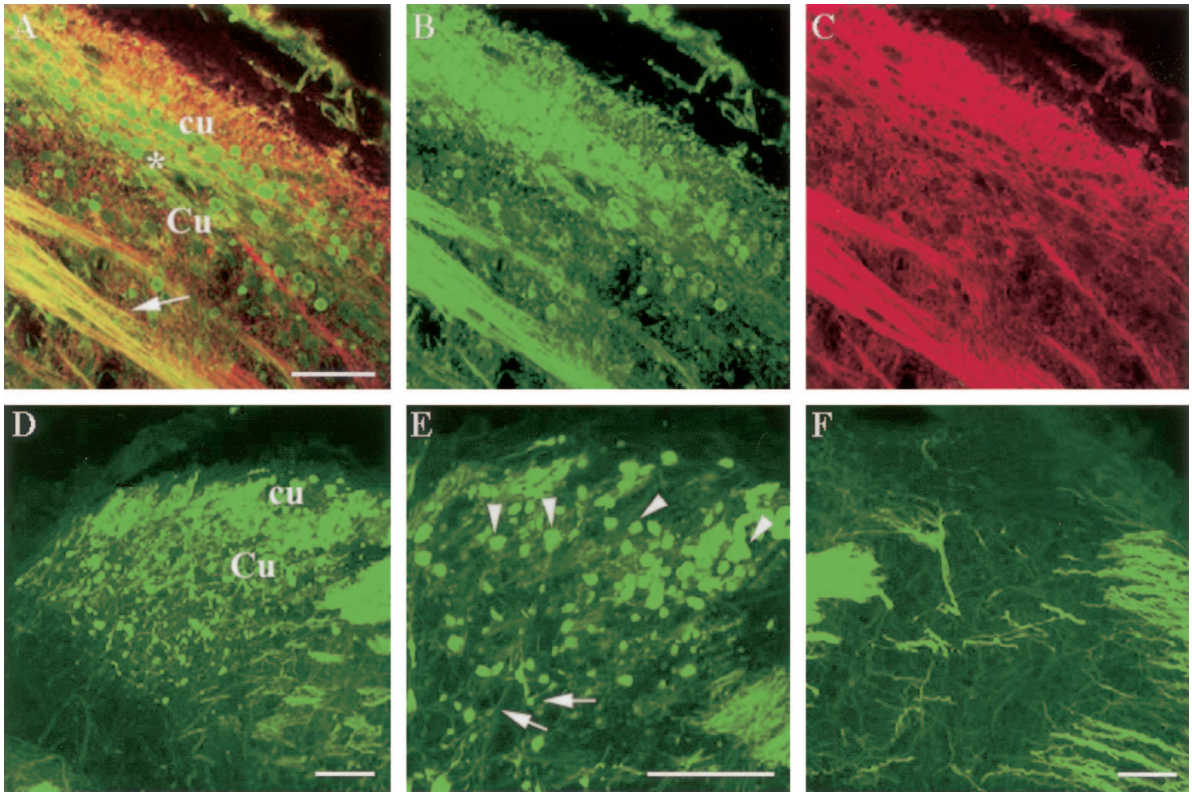

Figure 5. Expression of NF (green, **A–F**) and GAP43 (red, **A–C**) in the dorsal column in *Ndn*^{tm2Stw} mice during development. **A–C:** Sagittal section of E18 cuneate nucleus (Cu) and fasciculus (cu). Note the lack of co-localization within the dystrophic structures in the dorsal column (**asterisk**) and the complete co-localization in the tangential axons ventral to the Cu (**arrow**). **D** and **E:** Transverse section of Cu at E15 (**E**, detail from **D**). Dystrophic structures are present as early as E15 in Cu. Note that dystrophic structures (**arrowheads**) are larger than axonal growth cones (**arrows**). **F:** Transverse section of the putative area of the Cu at E13. There is no evidence of dystrophic structures at this time of development. Scale bars, 50 μm (**A–F**).

motor column with antibodies against the calcium-binding proteins parvalbumin (PV), calretinin (CR), and calbindin 28 kd (CB) was performed (Figure 6). In wild-type mice, PV immunoreactivity was present in cell bodies and fibers within both gracile and cuneate nuclei (Figure 6B). Intense fine and punctate staining (~5 μm diameter) was also present at the level of the vestibular nuclei and in scattered immunopositive cells within the ventrolateral medulla. In *Ndn*^{tm2Stw} mice, PV immunostaining was present in a similar pattern, but, notably, the abnormal structures immunolabeled with NF were immunopositive for PV as well (Figure 6, E and F). Double-labeling experiments with NF showed that the majority of NF aggregates were also PV-positive (Figure 6J).

In both wild-type and *Ndn*^{tm2Stw} mice, CR and CB immunoreactivity within the cuneate and gracile nuclei was present in several cells and in some fibers, the majority of which were small in size (Figure 6; C, D, G, and H); CR labeling was present in small caliber fibers and only occasionally in large NF-positive spheroids in *Ndn*^{tm2Stw} mice (Figure 6K). A few intensely CB-positive spheroids were present at the dorsal surface of the nucleus in *Ndn*^{tm2Stw} mice but they did not co-localize with NF (Figure 6L). Further, transverse sections labeled for NF and counterstained with Hoechst 33342 showed that, where NF accumulation occurred, no sign of neuronal degeneration was present and the abnormal staining was not associated with degenerated neuronal nuclei (Figure 6I).

A more detailed analysis of these spheroid structures at the electron microscope (Figure 7) showed that NF labeling was present in several small caliber axons that had similar morphology in wild-type and *Ndn*^{tm2Stw} mice (Figure 7, A and B). Intense immunolabeling was also present in abnormal structures exclusively identified in the *Ndn*^{tm2Stw} mice. These structures were larger than primary sensory afferents (5 to 10 μm) and contained several mitochondria that were swollen, dysmorphic, and embedded in large vacuoles (Figure 7; D to G, arrowheads). These structures were rarely associated with synaptic terminals (Figure 7G, asterisk).

Gracile and cuneate nuclei receive PV-positive primary afferents from the dorsal root ganglia through gracile and cuneate fasciculi and subsequently project to the thalamus and cortex through the medial lemniscus pathway to process proprioceptive information. As previously shown in Figure 2, the area of the medial lemniscus showed a reduced density of longitudinal fibers through the medulla. To further investigate the specificity of the defect in this system, we analyzed NF immunoreactivity in the dorsal root ganglia and in the thalamus. There was disarrangement of fibers and the presence of few dystrophic structures also in the dorsal root ganglia of *Ndn*^{tm2Stw} mice (data not shown). At the level of the thalamus,

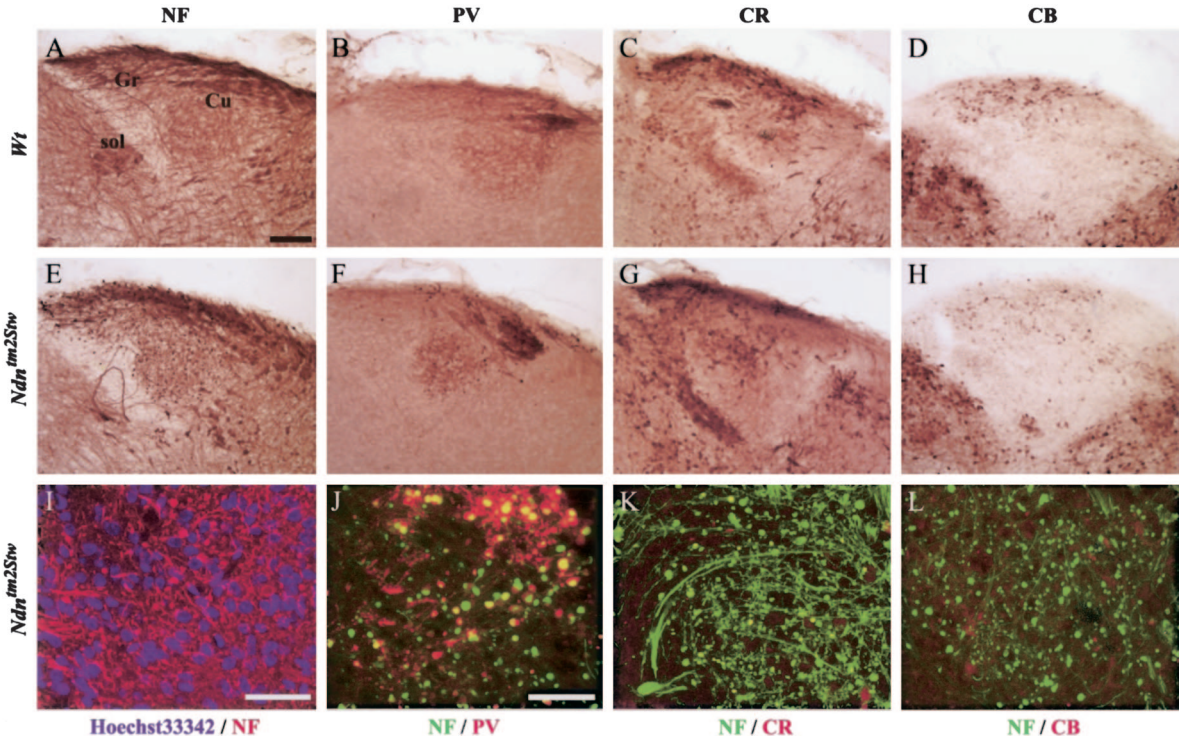

Figure 6. Calcium-binding proteins in the medullary dorsal column in E18 wild-type (**A–D**) and *Ndn*^{tm2Stw} mice (**E–L**). Immunolabeling for NF (**A**, **E**), PV (**B**, **F**), CR (**C**, **G**), and CB (**D**, **H**) in the dorsal column. Double immunolabeling for NF/Hoechst 33342 (**I**), NF/PV (**J**), NF/CR (**K**), and NF/CB (**L**) in the cuneate nucleus (Cu) of *Ndn*^{tm2Stw} mice. Dystrophic structures are identified by immunolabeling with NF and PV (**J**); they rarely express CB or CR (**K**, **L**). No Hoechst 33342-positive nuclei are present in the dystrophic structures. Gr, gracile nucleus; sol, solitary tract. Scale bars: 100 μm (**A–H**); 50 μm (**I–L**).

dystrophic structures were present in the mutants, not only at the level of the ventral posterior thalamic nucleus, where the majority of the proprioceptive pathway from the cuneate and gracile nuclei project, but also in several other thalamic nuclei. The cross-sectional area of the dystrophic structures in *Ndn*^{tm2Stw} mice was 16.06 $\pm$ 0.32 μm^2 compared to the normal cross-sectional area of 3.61 $\pm$ 0.49 μm^2 in wild-type animals. We did not perform a systematic study of other CNS structures, but did note similar defects within other brain structures in the vicinity of the thalamus (ie, septum, stria medullaris, anterior commissure, and dorsolateral geniculate nucleus).

Ontogeny of Medullary Cytoarchitecture in Ndn^{tm2Stw} *Mice*

To determine whether the abnormalities observed at E18 were due to a neurodegenerative process or a consequence of abnormal cell migration and axonal extension, we examined the expression of NF and GAP43 during early stages of development in the brainstem (Figure 8). At E14, NF-positive fibers and GAP43-positive growing axons were reduced in size throughout the medulla in *Ndn*^{tm2Stw} mice (data not shown). Longitudinal ascending and descending axon bundles were shrunk, disarranged, and defasciculated as observed at later developmental stages. The defects were also apparent in *Ndn*^{tm2Stw} mice at E10 (data not shown) and E11 (Figure 8). These results are consistent with necdin having a critical role in axonal organization and fasciculation and that its absence affects very early stages of neural development at the level of the brainstem.

General Cytoarchitectural Features in the Spinal Cord of Ndn^{tm2Stw} *Mice*

To further assess the extent of anatomical abnormalities within the developing CNS, we analyzed the main cytoarchitectural and anatomical features of the cervical spinal cord from E10 to E18 in *Ndn*^{tm2Stw} mice. In the E18 cervical spinal cord, spheroids were evident in lamina II and III and in the region ventral to the cuneate and gracile fasciculi and a few dystrophic structures were present in the ventral horn. The spheroids were similar to those detected at the level of the dorsal column in the brainstem (Figure 9, A and B) and they were detectable as early as E15 (Figure 9D). However, spheroids directly within the cuneate and gracile fasciculi were very rare. At E18, there was also a reduction in thickness of the anterolateral funiculus and the gracile and cuneate fasciculi (Figures 9 and 10). This phenomenon was present at earlier stages of development (E15 and E13) where NF-positive funiculi were reduced in size in *Ndn*^{tm2Stw} mice in comparison to wild-type mice (Figure 9, D and H, arrows) and several irregular bundles in the laminae IV to VII of the spinal cord were observed (Figure 9D). GAP43 immunolabeling showed a similar pattern of fiber distribution in *Ndn*^{tm2Stw} mice; a reduced size of longitudinal oriented funiculi (Figure 9F, arrow) and several immunopositive bundles in the central laminae (Figure 9F).

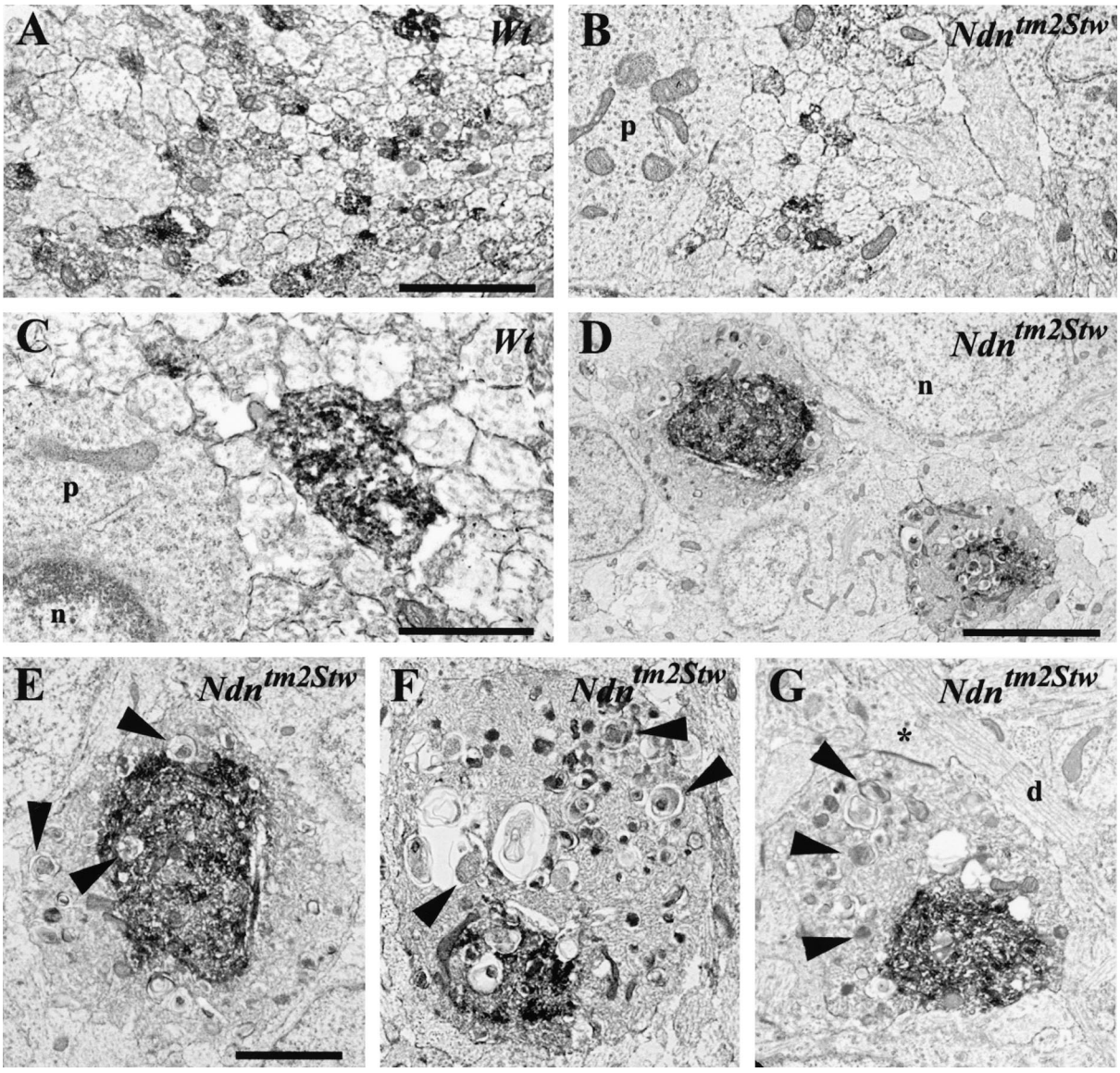

Figure 7. Ultrastructural analysis of the dorsal column in wild-type (**A**, **C**) and *Ndn*^{tm2Stw} mice (**B**, **D–G**). In both wild-type and *Ndn*^{tm2Stw} mice, small caliber axons are immunopositive for NF (**A–C**). In *Ndn*^{tm2Stw} mice, NF immunolabeling is also present in enlarged fibers, in which there is accumulation of NFs, a large number of mitochondria, and dark vesicles. Mitochondria are often swollen, dysmorphic, and embedded in large vacuoles (**arrowheads**). Note the presence of a synaptic terminal in **G** (**asterisk**). d, dendrite; n, nucleus; p, perykarion. Scale bars: 2 μm (**A**, **B**, **E–G**); 1 μm (**C**); 5 μm (**D**).

Further analysis on spinal cord structures was performed: both anterolateral funiculus and the cuneate and gracile fasciculi were analyzed and their areas measured at the cervical level of spinal cord. At E18, there was a significant reduction in size for both anterolateral funiculus (38 ± 2.2%) and dorsal fasciculus (18 ± 2.7%) in the *Ndn*^{tm2Stw} mice. We also obtained measurements of the area of the anterolateral funiculus during development and the reduction in this area was present at E13 (44 ± 2.7%), E14 (41 ± 2.1%), and E15 (38 ± 2.1%). The dorsal fasciculus was reduced also at E15 (40 ± 13.7%).

Figure 10 illustrates the organization of the developing spinal cord at the early stages of development (E10 and E11). To test the hypothesis that necdin deficiency could affect axonal extension and fasciculation in the spinal cord, we analyzed the development of commissural neurons and their axonal extension in the cervical spinal cord, a system that has been well studied and characterized.[53–55] Commissural neurons are generated in the dorsal spinal cord and send projections ventrally toward the floor plate. Subsequently they cross the midline and run longitudinally to their final targets along the ventral and lateral funiculi. This process is highly regulated by several chemoattractant and chemorepellant cues produced by the floor plate that interact with their specific receptors temporally expressed by the growth cone of commissural neurons.[56–58] In their initial growth toward the midline a subset of commissural axons express TAG1[59]; once the axons crossed the midline, TAG1 is down-regulated and they start expressing high levels of the adhesion molecule L1.[20] We therefore analyzed this subset of commissural axons during their extension process. At E10, TAG1 antibody labeled dorsal commissural neurons and commissural axons as they grew ventrally

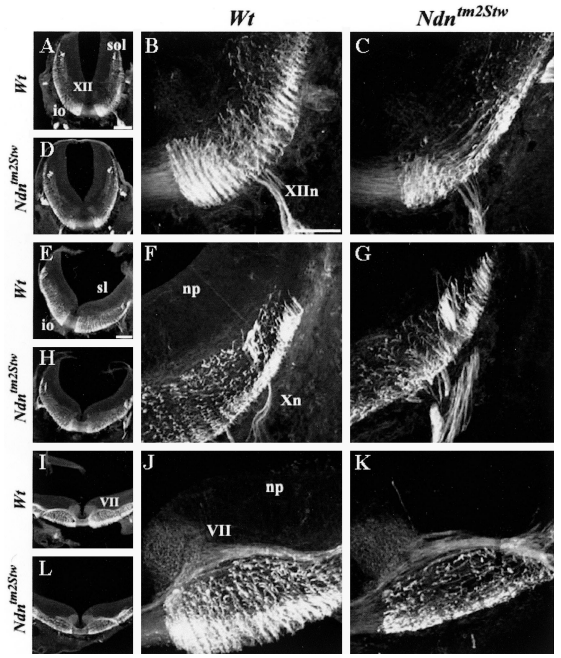

Figure 8. GAP43 expression at different caudo-rostral level of the brainstem in wild-type (**A**, **B**, **E**, **F**, **I, J**) and *Ndn*^{tm2Stw} mice (**C**, **D**, **G**, **H**, **K**, **L**) at E11. **A–D:** Caudal medulla at the level of the caudal inferior olive (io) domain and hyoglossal nucleus and nerve root (XII, XIIn). **B** and **C** are details from **A** and **D**, respectively. **E–H:** Rostral medulla at the rostral level of the inferior olive domain. **F** and **G** are details from **E** and **H**, respectively. **I–L:** Rostral medulla, **K** and **L** are details from **I** and **J**, respectively. Note the reduction in number of GAP43-immunopositive axons through the brainstem in *Ndn*^{tm2Stw} mice. Xn, vagus nerve root; np, neuroepithelium; sl, sulcus limitans; sol, solitary tract. Scale bars: 200 μm (**A**, **D**, **E**, **H**, **I**, **L**); 100 μm (**B**, **C**, **F**, **G**, **J**, **K**).

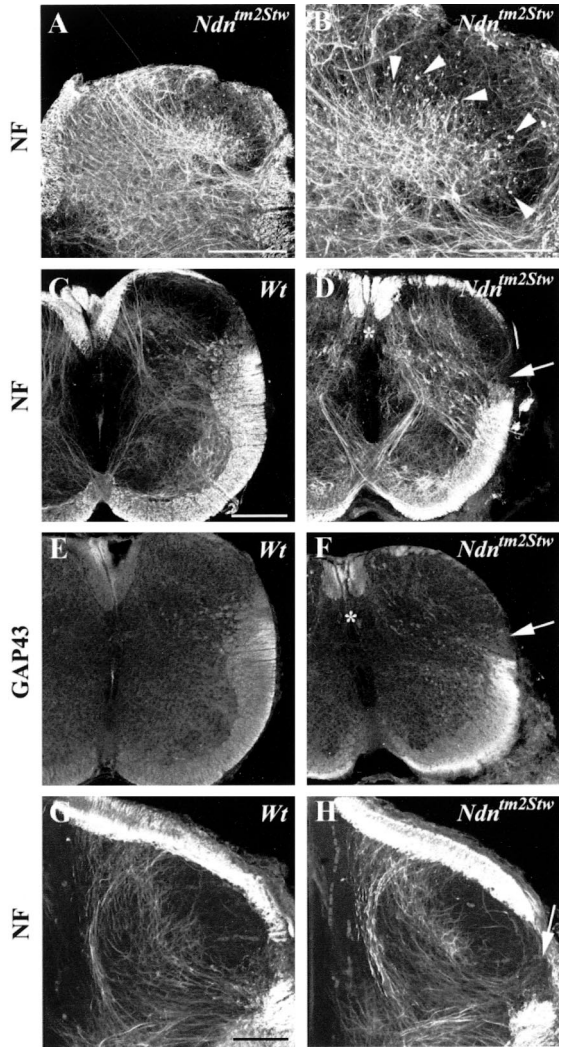

Figure 9. Expression of NF (**A–D**, **G**, **H**) and GAP43 (**E–F**) in the cervical spinal cord of wild-type (**C**, **E**, **G**) and *Ndn*^{tm2Stw} (**A**, **B**, **D**, **F**, **H**) mice. **A** and **B:** NF expression in the dorsal horn of E18 *Ndn*^{tm2Stw} mice shows dystrophic structures in laminae II and III of the spinal cord (**arrowheads**). **C–F:** NF and GAP43 expression in wild-type and *Ndn*^{tm2Stw} mice at E15. Note the reduction in size of the gracile and cuneate fasciculi in the dorsal spinal cord (**asterisks**) and the limited extension of the lateral funiculus in *Ndn*^{tm2Stw} mice (**arrows**). **G** and **H:** NF expression in dorsal horn of wild-type and *Ndn*^{tm2Stw} mice at E13. Scale bars: 200 μm (**A**, **C–F**); 100 μm (**B**, **G**, **H**).

toward the floor plate and as they crossed to the contralateral side (Figure 10, A and C). GAP43 was up-regulated at the level of the floor plate and the nerves extending out from the spinal cord. No major differences were detected between wild-type and *Ndn*^{tm2Stw} mice both at the level of the dorsal commissural neurons and the floor plate (Figure 10, B and D).

At E11, NF antibody labeled the numerous axons and cell bodies present in the spinal cord and the dorsal root ganglia. The ventral and lateral funiculi were compact and strongly immunoreactive for NF in wild-type animals. In *Ndn*^{tm2Stw} mice funiculi were thinner than in wild-type mice and the extension of the lateral funiculi was reduced toward the dorsal spinal cord (Figure 10, E and I, arrow). At this stage of development, most of the commissural axons have crossed the midline and the expression of TAG1 was clearly down-regulated in both wild-type and *Ndn*^{tm2Stw} mice (Figure 10, F and J); GAP43 was strongly expressed in the ventral and lateral funiculi in wild-type mice (Figure 10G). L1, the adhesion molecule expressed by commissural axons on crossing the midline,[59] was expressed along the ventral and lateral funiculi in wild-type mice whereas both L1- and GAP43-immunopositive fibers in *Ndn*^{tm2Stw} mice were reduced in the ventral funiculus and almost absent at the dorsal level of the lateral funiculus (Figure 10, K and L, arrows). These results suggest that as early as E13 to E15 there are major defects in the spinal cord within the longitudinally oriented fibers of neurons generated at either rostral or caudal locations of the CNS (mainly at the level of the anterolateral funiculus) or at the level of DRGs (dorsal fasciculus and anterolateral system).

Main Cytoarchitectural Features in Ndn^{tm2Stw} *Mouse Diaphragm*

To determine whether the abnormalities present in subsets of axonal bundles within the medulla and spinal cord were also present peripherally, we compared the phrenic branching pattern in wild-type and *Ndn*^{tm2Stw} mice. The intramuscular branching of the phrenic nerve within the perinatal rodent diaphragm muscle is very regular with a characteristic trifurcating pattern[60] and thus particularly suitable for such analysis. As shown in Figure 11, NF labeling shows the phrenic innervation in the diaphragm

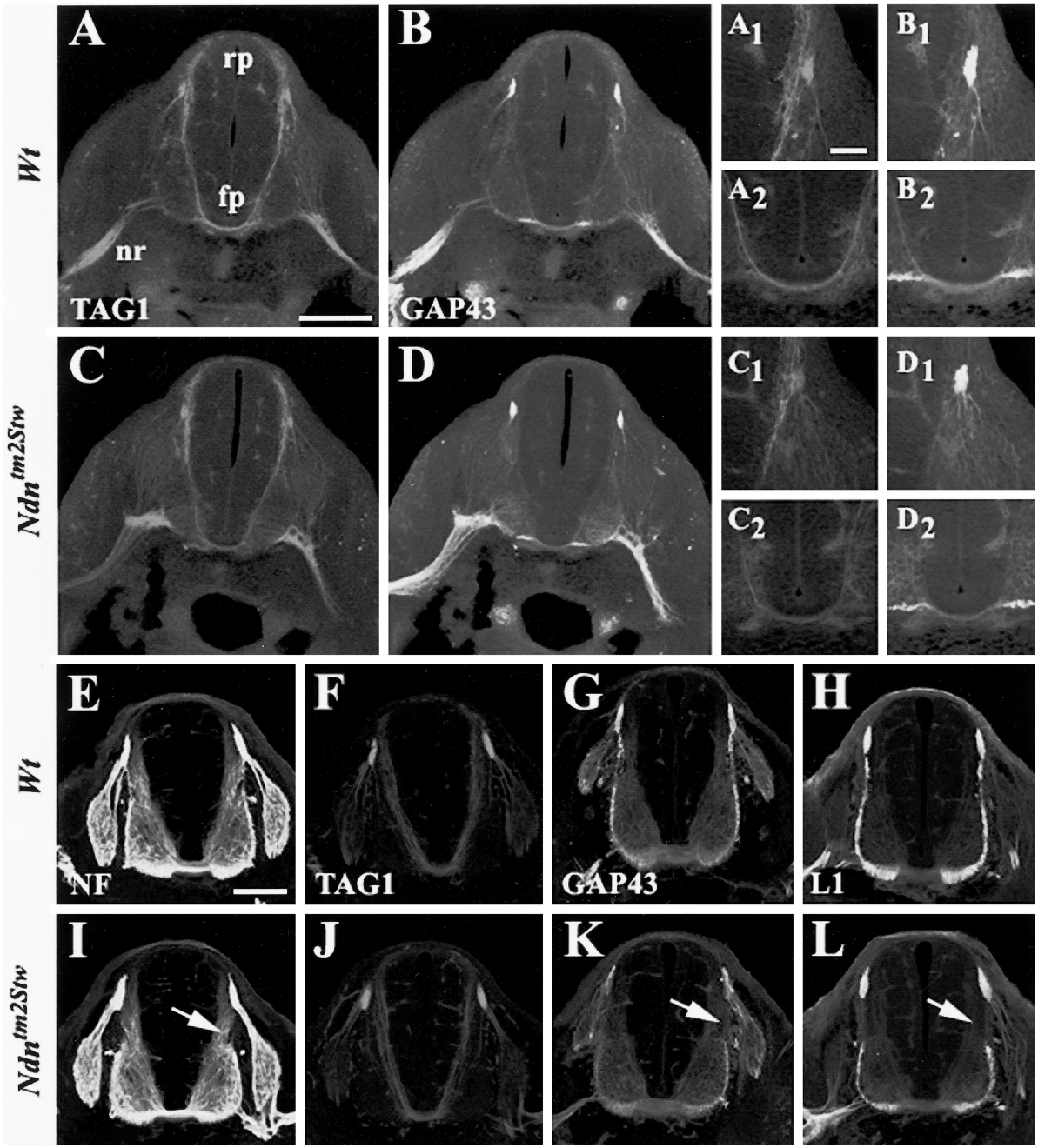

Figure 10. Expression of TAG1, GAP43, NF, and L1 in cervical spinal cord of wild-type (**A**, **B**, **E–H**) and *Ndn*^{tm2Stw} (**C**, **D**, **I–L**) mice at E10 (**A–D**) and E11 (**E–L**). **A**, **C**, **F**, and **J:** TAG1 expression in cervical spinal cord at E10 and E11. **A1**, **A2**, and **C1**, **C2** are details of commissural neurons and ventral midline from **A** and **C**, respectively. **B**, **D**, **G**, and **K:** GAP43 expression in cervical spinal cord at E10 and E11. **B1**, **B2**, and **D1**, **D2** are details of commissural neurons and ventral midline from **B** and **D**, respectively. **E** and **I:** NF expression in cervical spinal cord at E11. **H** and **L:** L1 expression in cervical spinal cord at E11. No major differences between wild-type and *Ndn*^{tm2Stw} mice were identified by TAG1 and GAP43 immunolabeling at E10. At E11, TAG1 immunolabeling does not show any major differences between wild-type and *Ndn*^{tm2Stw} mice through the spinal cord; NF-, GAP43-, and L1-immunopositive axons are reduced in *Ndn*^{tm2Stw} mice at the level of the lateral funiculus (**arrows**). fp, floor plate; rp, roof plate; nr, nerve root. Scale bars: 200 μm (**A–L**); 50 μm (**A1–D2**).

of wild-type and *Ndn*^{tm2Stw} mice. The phrenic nerve successfully innervated the diaphragm in the *Ndn*^{tm2Stw} mice an EMG signal could be recorded from the diaphragm muscle (shown in Figure 12). However, the orientation of the secondary intramuscular branches in *Ndn*^{tm2Stw} mouse diaphragms was clearly irregular in comparison to the orderly pattern observed in the wild type. This included abnormalities in the orientation and extent of axon trajectories (Figure 11, A and B, asterisk) within the muscle and the tightness of axon fasciculation (Figure 11, C and D).

Electrophysiological Recordings of Respiratory Rhythm Generated by Ndn^{tm2Stw} *Mice*

The respiratory rhythm generated by *in vitro* preparations isolated from *Ndn*^{tm2Stw} mice is unstable (Figure 12).

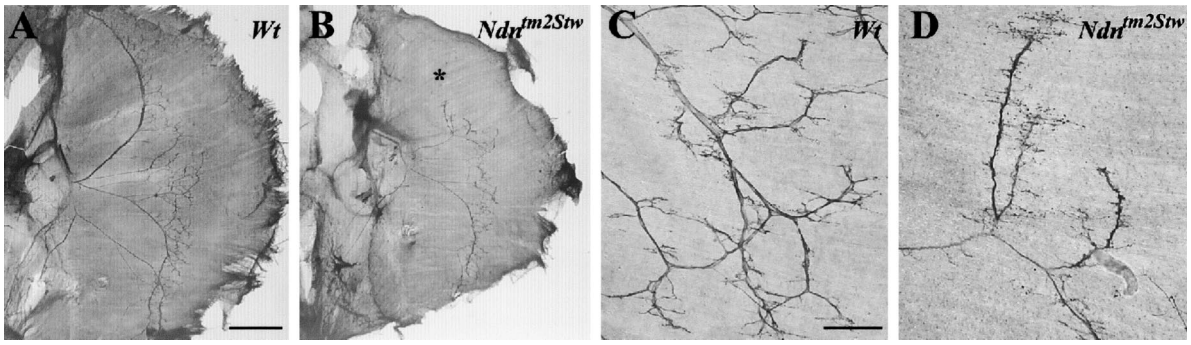

Figure 11. Diaphragm innervation of wild-type (**A**, **C**) and *Ndn*^{tm2Stw} (**B**, **D**) mice at E16. NF immunolabeling shows the reduced extension (**asterisk** in **B**) and innervation of the phrenic nerve intramuscular branching within the diaphragm of mutant mice. There was no evidence of swollen axons or dystrophic structures at phrenic nerve terminals. Scale bars: 2 mm (**A**, **B**); 200 μm (**C**, **D**).

There were prominent bouts of respiratory depression and apneas during which the frequency of inspiratory bursts was typically less than one per minute. The bouts of suppressed respiratory rhythmic discharge (lasting 16 ± 7 minutes, $n = 13$) were interspersed with periods of inspiratory motor bursts close to frequencies observed in wild-type preparations (lasting 7.5 ± 3.4 minutes, $n = 13$). As shown by the long duration recording in Figure 12 (~2 hours), there was a clear periodicity to the fluctuations between slow and fast rhythms that was prominent in all brainstem-spinal cord preparations examined.

We tested the hypothesis that the respiratory rhythm could be normalized in the presence of endogenously applied neurotransmitter agonists (SubP and TRH) known to excite neurons within the preBötC region.[61,62]

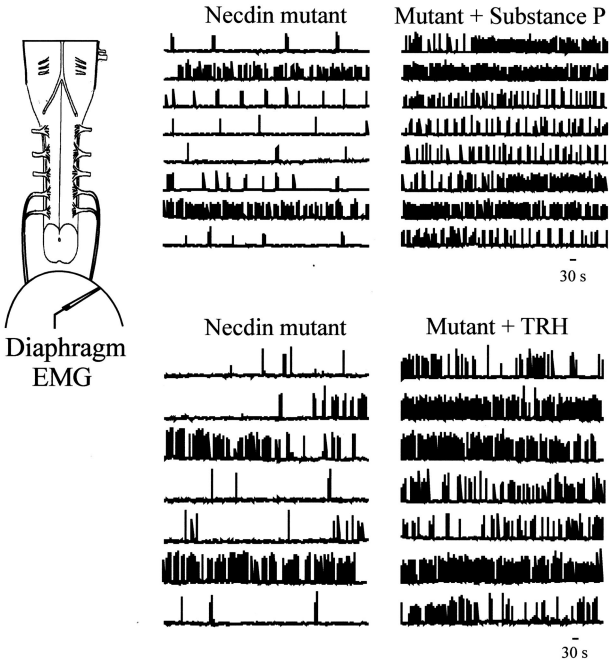

Figure 12. Effects of excitatory neuromodulators on respiratory rhythm generated by *Ndn*^{tm2Stw} mouse brainstem-spinal cord preparations. **Left**: The isolated brainstem-spinal cord-diaphragm *in vitro* preparation. **Right**: Rectified and integrated suction electrode recordings of diaphragm EMG from E18.5 *Ndn*^{tm2Stw} mice in control solution (**left**) and in response to the addition of SubP (1 μm) and TRH (1 μm) to the bathing medium (**right**). Both neuromodulators increased the overall frequency of respiratory rhythm but the instabilities in the frequency remained.

As shown in Figure 12, addition of SubP (1 μmol/L) and TRH (1 μmol/L) significantly modulated the rhythm generated by *Ndn*^{tm2Stw} mouse brainstem-spinal cord preparations. The frequency of discharge during the previously slow periods was increased markedly and the incidence of apneas diminished. However, the fluctuations in respiratory frequency between slow and fast rhythmogenesis persisted. The application of SubP (1 μmol/L) to medullary slice preparations had similar modulatory effects (data not shown). Further, exogenous application of serotonin (25 μmol/L) or noradrenaline (3 to 30 μmol/L) resulted in the same excitatory response (data not shown). Thus, we concluded that addition of appropriate neuromodulatory drive to the preBötC region could alleviate the long periods of slow respiratory rhythms and apnea, however, the overall respiratory rhythm instability persisted.

We also tested the actions of growth hormone due to the fact that it is effective in alleviating apnea in PWS infants.[8] The stimulatory effects of growth hormone observed clinically are likely not due to direct stimulation of the preBötC because endogenous application (1 to 15 nmol/L) did not affect respiratory frequency in either wild-type or mutant *in vitro* preparations. Neither did insulin-like growth factor-1 (10 to 40 nmol/L), an intermediate effector of growth hormone action, have any noticeable effect on respiratory neural discharge *in vitro*.

Discussion

Mouse models with selective gene deletions in chromosomal region 7C have been generated for analyses of the pathogenesis underlying PWS. Despite some variability in the phenotype among the different generated necdin-null mouse models,[15–17] correspondence with clinical manifestations of PWS are present. The neuronal mechanisms underlying the defects in genetic models have been elusive. Past studies using general histological markers of brain sections revealed no obvious differences in necdin-null mice outside of a reduction of oxytocin- and luteinizing hormone-releasing hormone-expressing neurons in the hypothalamus.[16] In this study, we performed a more detailed examination to determine whether there were widespread developmental abnor-

malities of CNS structure. Particular attention was initially directed to the developing medulla due to its importance in generating respiratory rhythm, an aspect that is severely compromised in *Ndn*^{tm2Stw} mice[18] and which may be of relevance to neonatal central apneas associated with PWS. We extended the investigation to the spinal cord, diaphragm, and sensory pathways to further elucidate the extent of the developmental anomalies.

Thionine staining and immunolabeling for NF demonstrated anatomical abnormalities within the medulla. The defects included defasciculation of axonal tracts, aberrant neurite processes, a reduced size of the some motoneuronal pools (X, XII, and NA), and most notably, a major defect in the cytoarchitecture of the cuneate/gracile nuclei and their fasciculi. Further, NF immunolabeling demonstrated that the majority of axonal tracts within the medulla were abnormal in *Ndn*^{tm2Stw} mice. Axonal bundles were reduced in size, they appeared defasciculated and distributed in an irregular pattern. The differences in axonal patterning between wild-type and *Ndn*^{tm2Stw} mice were present from the time when the first axonal tracts generated from postmitotic neurons migrated toward their targets. Further, the reduction in the size of motor nuclei appeared very early in development and thus could not be explained simply by an increase in apoptosis. The presence of disarrangement of the radial glia during the development of the brainstem may suggest a larger role for necdin in axonal patterning and orientation. Further studies will be necessary to address the relative role and interactions between radial glia and extending axons in *Ndn*^{tm2Stw} mice. Defects in axonal fasciculation and extension were also present in a subset of spinal neurons and within phrenic nerve intramuscular branches. These results suggest that the anatomical defects in *Ndn*^{tm2Stw} mice are more widespread than previously appreciated.

Respiratory-Related Defects within the Medulla

An area of particular interest within the medulla was the preBötC, the putative site for rhythmogenesis of inspiratory drive.[63] A detailed understanding of the cellular mechanisms underlying rhythm and pattern generation with the preBötC is a major focus of ongoing studies. To date, there are data to support a pacemaker-network hypothesis that states that the kernel for rhythm generation consists of a population of neurons with intrinsic pacemaker properties that are embedded within, and modulated by, a neuronal network.[64,65] The primary conditioning excitatory drive that maintains the oscillatory state arises from activation of glutaminergic receptors.[66,67] Additional conditioning synaptic drive is provided by a diverse group of neuromodulators including GABA, 5HT, TRH, noradrenaline, opioids, prostaglandins, SubP, and acetylcholine.[68–70] Contrary to our initial hypothesis, the gross structure of the preBötC was normal in *Ndn*^{tm2Stw} mice, as shown by the presence of NK1R- and SST-immunopositive neurons within the putative region of the preBötC. Rather, there were clear anatomical abnormalities in surrounding medullary structures that provide conditioning synaptic input to respiratory rhythmogenic neurons. Several TH-immunopositive neurons within the medulla were swollen and irregularly distributed in ectopic areas. Further, TH-immunopositive fibers in the ventral bundles and in the ventral medulla were enlarged. Abnormal morphology and orientation of fibers within the ventrolateral medulla was also observed within incoming axons labeled for SubP and 5HT. The abnormal morphology of neuronal fibers expressing various neurotransmitters suggests that the absence of necdin determines a defect in the formation and the morphology of axonal tracts and fibers within the medulla in different neuronal phenotypes that regulate preBötC function.

Brainstem-spinal cord and medullary slice preparations from *Ndn*^{tm2Stw} mice showed irregular respiratory activity associated with several periods of apneas and respiratory depression. The frequency of the respiratory rhythm could be increased and periods of apnea alleviated by the administration of SubP, TRH, 5-HT, and noradrenaline. However, the fluctuations in the respiratory frequency continued in the *Ndn*^{tm2Stw} mice. Our interpretation is that the endogenous application of neuromodulators overcame much of the deficit resulting from the abnormalities in medullary structures that normally provide conditioning drive to the preBötC. An abnormality in the function of the preBötC per se remains, however. The functional defect could reflect changes in neuronal properties or abnormalities in the preBötC network connectivity due to problems with axon guidance and fasciculation.

Defects within Gracile and Cuneate Nuclei

The most remarkable anatomical medullary defects in *Ndn*^{tm2Stw} mice were observed in the gracile and cuneate nuclei. Enlarged, dystrophic structures, identified via NF and PV immunolabeling, were abundant in the area. There was no evidence of neuronal cell death or reactive astrocytes in the dystrophic region. Rather, the dystrophic structures were similar in appearance to those previously reported for degenerating primary afferents.[70–74] Further, the dystrophic structures were similar to what has been reported in association with defects in kinesin-mediated axonal transport and outgrowth within the *Drosophila* CNS.[75,76] Similar phenomena have been previously identified in normal aging rodents[74,77] and in the early postnatal life of animal models for Niemann-Pick disease[71,78] and for gracile axonal dystrophy.[70] In those models, degenerating primary afferent fibers are the consequence of either a deficit in lipid storage metabolism[79] or abnormal transport and protein accumulation of amyloid β-protein and ubiquitin-positive deposits.[80,81] Ultrastructural analysis of the dorsal column via electron microscopy demonstrated that the abnormal structures were packed with NF and mitochondria, some of which had an abnormal morphology. The abnormalities detected in the dorsal column may represent the initial steps of axonal degeneration in the distal ends of primary ascending afferent axons or the consequence of an abnormal axonal function that disrupts axonal outgrowth and

homeostasis. This hypothesis is supported by the fact that dystrophic structures were consistently more evident at the level of the medulla rather than along the dorsal funiculi in the spinal cord and in the DRGs. Further studies will be necessary for clarifying the mechanism of this phenomenon and the role that necdin plays. Given the specific distribution of dystrophic structures and the differences in size from other enlarged fibers immunopositive for SubP and 5HT in the ventrolateral medulla, we also propose that these phenomena are different, even though they are both determined by the absence of necdin during development.

Spinal Cord and Diaphragm Defects

An analysis of spinal cord development indicated that in *Ndn*^{tm2Stw} mice most of the axonal tracts initially formed normally. However, there were indications of abnormalities in the dorsal column and in the anterolateral funiculus. The reduced size of these axonal tracts and the presence of dystrophic structures in the dorsal horn correlated with the defects observed in the upper structures (gracile and cuneate nuclei and reticular formation) and suggest a deficiency in the proper development of longitudinally projecting axons in the dorsal column and the anterolateral funiculus. Further studies (eg, dye tracing) will be necessary to clarify if specific tracts in the anterolateral funiculus are affected or if a more general defect is present in these fibers. Further, anterograde dye tracing could clarify if the reduced extension is proportionally related to either a reduction in number of neurons that send projections to different levels of the spinal cord or a reduction in the number of fibers extending to the spinal cord, or both.

Axons exiting the spinal cord within ventral roots appeared grossly normal although motoneuron pools were reduced in size (data not shown). Further, there were clear abnormalities of the fine intramuscular branching pattern of the phrenic nerve within the diaphragm muscle. Previous preliminary data[82] reported abnormalities in the density and localization of acetylcholine receptors in the diaphragm of *Ndn*^{tm2Stw} mice. These subtle, yet significant, abnormalities in the motor system may be associated with the prominence of hypotonia in infants with PWS.

Potential Mechanisms Underlying Pathogenesis

The functional roles of necdin, which is expressed widely within the developing CNS, remain to be clearly delineated. However, potential regulatory actions of necdin have been derived from *in vitro* studies in which necdin expression was induced in proliferative cell lines or blocked by anti-sense oligonucleotides in cultured dorsal root ganglion neurons.[83–86] Collectively, those data suggest that necdin interacts with cytoplasmic and nuclear proteins to control cell growth, proliferation, and apoptosis. More recent studies using heterologous expression systems have demonstrated an interaction between necdin and fasciculation and elongation (Fez) proteins implicated in centrosome-mediated cytoskeletal rearrangement after neuronal differentiation and in axonal outgrowth.[87] These data support a model whereby upregulation of necdin in postmitotic neurons stabilizes Fez proteins to facilitate centrosome-mediated cytoskeletal rearrangements required for axonal outgrowth and kinesin-mediated transport. The abnormalities in neuronal migration and the extension, arborization, and fasciculation of axons during early stages of development reported here in the detailed analysis of *Ndn*^{tm2Stw} mice are consistent with the hypothesized roles for necdin. However, it is important to note that only certain axonal tracts and neuronal populations are clearly affected whereas others appear normal in the mouse model.

Relevance to PWS

Dysfunction of various hypothalamic systems, as evident from histological examination of postmortem brain tissue, may be the basis of a number of symptoms in PWS.[88] Other reported CNS deficits within PWS patients include enlarged lateral ventricles, hypoplasia of the corpus callosum, abnormal cortical development, and some irregularities in the structures of inferior olive, dentate nucleus, and cerebellum.[89–91] In light of the results from this current study it will be important to perform more extensive and detailed examinations of the CNS in PWS patients for evidence of the types of more subtle defects demonstrated in the necdin-null model. Axonal defasciculations, abnormalities of neurite extension, and reduced numbers of neurons within specific nuclei could be involved in some of the cognitive, behavioral, somatosensory, and respiratory deficits associated with PWS.

Acknowledgments

We thank Honey Chan for technical assistance with electron microscopy and Syann Lee for input into preliminary stages of the study.

References

1. Goldstone AP: Prader-Willi syndrome: advances in genetics, pathophysiology and treatment. Trends Endocrinol Metab 2004, 15:12–20
2. Stevenson DA, Anaya TM, Clayton-Smith J, Hall BD, Van Allen MI, Zori RT, Zackai EH, Frank G, Clericuzio CL: Unexpected death and critical illness in Prader-Willi syndrome: report of ten individuals. Am J Med Genet 2004, 124A:158–164
3. Arens R, Gozal D, Omlin K, Livingston FR, Liu J, Keens TG, Ward SL: Hypoxic and hypercapnic ventilatory responses in Prader-Willi syndrome. J Appl Physiol 1994, 77:2224–2230
4. Gozal D, Arens R, Omlin KJ, Ward SL, Keens TG: Absent peripheral chemosensitivity in Prader-Willi syndrome. J Appl Physiol 1994, 77:2231–2236
5. Clift S, Dahlitz M, Parkes JD: Sleep apnoea in the Prader-Willi syndrome. J Sleep Res 1994, 3:121–126
6. Wharton RH, Loechner KJ: Genetic and clinical advances in Prader-Willi syndrome. Curr Opin Pediatr 1996, 8:618–624
7. Schluter B, Buschatz D, Trowitzsch E, Aksu F, Andler W: Respiratory control in children with Prader-Willi syndrome. Eur J Pediatr 1997, 156:65–68
8. Menendez AA: Abnormal ventilatory responses in patients with Prader-Willi syndrome. Eur J Pediatr 1999, 158:941–942

9. Manni R, Politini L, Ferrillo F, Livieri C, Veneselli E, Biancheri R, Martinetti M, Tartara A: Hyperinsomnia in the Prader Willi syndrome: clinical-electrophysiological features and underlying factors. Clin Neurophysiol 2001, 112:800–805
10. Nixon GM, Brouillette RT: Sleep and breathing in Prader-Willi syndrome. Pediatr Pulmonol 2002, 34:209–217
11. Nicholls RD, Knepper JL: Genome organization, function, and imprinting in Prader-Willi and Angelman syndromes. Annu Rev Genomics Hum Genet 2001, 2:153–175
12. Jay P, Rougeulle C, Massacrier A, Moncla A, Mattei MG, Malzac P, Roeckel N, Taviaux S, Lefranc JL, Cau P, Berta P, Lalande M, Muscatelli F: The human necdin gene NDN, is maternally imprinted and located in the Prader-Willi syndrome chromosomal region. Nat Genet 1997, 17:357–361
13. MacDonald HR, Wevrick R: The necdin gene is deleted in Prader-Willi syndrome and is imprinted in human and mouse. Hum Mol Genet 1997, 6:1873–1878
14. Sutcliffe JS, Han M, Christian SL, Ledbetter DH: Neuronally-expressed necdin gene: an imprinted candidate gene in Prader-Willi syndrome. Lancet 1997, 350:1520–1521
15. Gerard M, Hernandez L, Wevrick R, Stewart C: Disruption of the mouse necdin gene results in early postnatal lethality: a model for neonatal distress in Prader-Willi syndrome. Nat Genet 1999, 23:199–202
16. Muscatelli F, Abrous DN, Massacrier A, Boccaccio I, Moal ML, Cau P, Cremer H: Disruption of the mouse necdin gene results in hypothalamic and behavioral alterations reminiscent of the human Prader-Willi syndrome. Hum Mol Genet 2000, 9:3101–3110
17. Tsai TF, Armstrong D, Beaudet AL: Necdin-deficient mice do not show lethality or the obesity and infertility of Prader-Willi syndrome. Nat Genet 1999, 22:15–16
18. Ren J, Lee S, Pagliardini S, Gerard CL, Stewart CL, Greer JJ, Wevrick R: Absence of Ndn, encoding the Prader-Willi syndrome-deleted gene necdin, results in congenital deficiency of central respiratory drive in neonatal mice. J Neurosci 2003, 23:1569–1573
19. Kaufman MH: The Atlas of Mouse Development. London, Academic Press, 1994
20. Dodd J, Morton SB, Karagogeos D, Yamamoto M, Jessell TM: Spatial regulation of axonal glycoprotein expression on subsets of embryonic spinal neurons. Neuron 1988, 1:105–116
21. Karlsson JE, Rosengren LE, Haglid KG: Polyclonal antisera to the individual neurofilament triplet proteins: a characterization using ELISA and immunoblotting. J Neurochem 1989, 53:759–765
22. Albers KM, Wright DE, Davis BM: Over-expression of nerve growth factor in epidermis of transgenic mice causes hypertrophy of the peripheral nervous system. J Neurosci 1994, 14:1422–1432
23. Meiri KF, Bickerstaff LE, Schwob JE: Monoclonal antibodies show that kinase C phosphorylation of GAP-43 during axonogenesis is both spatially and temporally restricted in vivo. J Cell Biol 1991, 112:991–1005
24. Alvarez-Buylla A, Buskirk DR, Nottebohm F: Monoclonal antibody reveals radial glia in adult avian brain. J Comp Neurol 1987, 264:159–170
25. Yamamoto M, Boyer AM, Crandall JE, Edwards M, Tanaka H: Distribution of stage-specific neurite-associated proteins in the developing murine nervous system recognized by a monoclonal antibody. J Neurosci 1986, 6:3576–3594
26. Vigna SR, Bowden JJ, McDonald DM, Fisher J, Okamoto A, McVey DC, Payan DG, Bunnett NW: Characterization of antibodies to the rat substance P (NK-1) receptor and to a chimeric substance P receptor expressed in mammalian cells. J Neurosci 1994, 14:834–845
27. Mantyh PW, Rogers SD, Honore P, Allen BJ, Ghilardi JR, Li J, Daughters RS, Lappi DA, Wiley RG, Simone DA: Inhibition of hyperalgesia by ablation of lamina I spinal neurons expressing the substance P receptor. Science 1997, 278:275–279
28. Shiromani PJ, Lai YY, Siegel JM: Descending projections from the dorsolateral pontine tegmentum to the paramedian reticular nucleus of the caudal medulla in the cat. Brain Res 1990, 517:224–228
29. Cuello AC, Galfre G, Milstein C: Detection of substance P in the central nervous system by a monoclonal antibody. Proc Natl Acad Sci USA 1979, 76:3532–3536
30. Millhorn DE, Hökfelt T, Seroogy K, Verhofstad AAJ: Extent of colocalization of serotonin and GABA in neurons of the ventral medulla oblongata in rat. Brain Res 1988, 461:169–174
31. Stornetta RL, Rosin DL, Wang H, Sevigny CP, Weston MC, Guyenet PG: A group of glutamatergic interneurons expressing high levels of both neurokinin-1 receptors and somatostatin identifies the region of the pre-Botzinger complex. J Comp Neurol 2003, 455:499–512
32. Pinault D, Smith Y, Dechenes M: Dendrodendritic and axoaxonic synapses in the thalamic reticular nucleus of the adult rat. J Neurosci 1997, 17:3215–3233
33. Smith JC, Greer JJ, Liu GS, Feldman JL: Neural mechanisms generating respiratory pattern in mammalian brain stem-spinal cord in vitro. I. Spatiotemporal patterns of motor and medullary neuron activity. J Neurophysiol 1990, 64:1149–1169
34. Greer JJ, Smith JC, Feldman JL: Respiratory and locomotor patterns generated in the fetal rat brain stem-spinal cord in vitro. J Neurophysiol 1992, 67:996–999
35. Smith JC, Ellenberger HH, Ballanyi K, Richter DW, Feldman JL: Pre-Bötzinger complex: a brainstem region that may generate respiratory rhythm in mammals. Science 1991, 254:726–728
36. Friedland DR, Eden AR, Laitman JT: Naturally occurring motoneuron cell death in rat upper respiratory tract motor nuclei: a histological, fast DiI and immunocytochemical study in the hypoglossal nucleus. J Neurobiol 1995, 27:520–534
37. Friedland DR, Eden AR, Laitman JT: Naturally occurring motoneuron cell death in rat upper respiratory tract motor nuclei: a histological, fast DiI and immunocytochemical study of the nucleus ambiguus. J Neurobiol 1995, 26:563–578
38. Dupouey P, Benjelloun S, Gomes D: Immunohistochemical demonstration of an organized cytoarchitecture of the radial glia in the CNS of the embryonic mouse. Dev Neurosci 1985, 7:81–93
39. Rakic P: Neuron-glia relationship during granule cell migration in developing cerebellar cortex. A Golgi and electronmicroscopic study in Macacus Rhesus. J Comp Neurol 1971, 141:283–312
40. Gray PA, Rekling JC, Bocchiaro CM, Feldman JL: Modulation of respiratory frequency by peptidergic input to rhythmogenic neurons in the preBotzinger complex. Science 1999, 286:1566–1568
41. Wang H, Stornetta RL, Rosin DL, Guyenet PG: Neurokinin-1 receptor-immunoreactive neurons of the ventral respiratory group in the rat. J Comp Neurol 2001, 434:128–146
42. Guyenet PG, Sevigny CP, Weston MC, Stornetta RL: Neurokinin-1 receptor-expressing cells of the ventral respiratory group are functionally heterogeneous and predominantly glutamatergic. J Neurosci 2002, 22:3806–3816
43. Blanchi B, Kelly LM, Viemari JC, Lafon I, Burnet H, Bevengut M, Tillmanns S, Daniel L, Graf T, Hilaire G, Sieweke MH: MafB deficiency causes defective respiratory rhythmogenesis and fatal central apnea at birth. Nat Neurosci 2003, 6:1091–1100
44. Pagliardini S, Ren J, Greer JJ: Ontogeny of the pre-Botzinger complex in perinatal rats. J Neurosci 2003, 23:9575–9584
45. Thoby-Brisson M, Cauli B, Champagnat J, Fortin G, Katz DM: Expression of functional tyrosine kinase B receptors by rhythmically active respiratory neurons in the pre-Botzinger complex of neonatal mice. J Neurosci 2003, 23:7685–7689
46. Viemari JC, Bevengut M, Burnet H, Coulon P, Pequignot JM, Tiveron MC, Hilaire G: Phox2a gene, A6 neurons, and noradrenaline are essential for development of normal respiratory rhythm in mice. J Neurosci 2004, 24:928–937
47. Huang ZG, Subramanian SH, Balnave RJ, Turman AB, Moi Chow C: Roles of periaqueductal gray and nucleus tractus solitarius in cardiorespiratory function in the rat brainstem. Respir Physiol 2000, 120:185–195
48. Errchidi S, Monteau R, Hilaire G: Noradrenergic modulation of the medullary respiratory rhythm generator in the newborn rat: an in vitro study. J Physiol 1991, 443:477–498
49. Hilaire G, Monteau R, Errchidi S: Possible modulation of the medullary respiratory rhythm generator by the noradrenergic A5 area: an in vitro study in the newborn rat. Brain Res 1989, 485:325–332
50. Pickel VM, Joh TH, Reis DJ: Ultrastructural localization of tyrosine hydroxylase in noradrenergic neurons of brain. Proc Natl Acad Sci USA 1975, 72:659–663
51. Celio MR: Calbindin D-28k and parvalbumin in the rat nervous system. Neuroscience 1990, 35:375–475
52. Crockett DP, Maslany S, Egger MD: Synaptophysin immunoreactivity and distributions of calcium-binding proteins highlight the functional organization of the rat's dorsal column nuclei. Brain Res 1996, 707:31–46

53. Strahle U, Lam CS, Ertzer R, Rastegar S: Vertebrate floor-plate specification: variations on common themes. Trends Genet 2004, 20:155–162
54. Dickson BJ: Molecular mechanisms of axon guidance. Science 2003, 298:1959–1964
55. Jessell TM: Neuronal specification in the spinal cord: inductive signals and transcriptional codes. Nat Rev Genet 2000, 1:20–29
56. Long H, Sabatier C, Ma L, Plump A, Yuan W, Ornitz DM, Tamada A, Murakami F, Goodman CS, Tessier-Lavigne M: Conserved roles for Slit and Robo proteins in midline commissural axon guidance. Neuron 2004, 42:213–223
57. Charron F, Stein E, Jeong J, McMahon AP, Tessier-Lavigne M: The morphogen sonic hedgehog is an axonal chemoattractant that collaborates with netrin-1 in midline axon guidance. Cell 2003, 113:11–23
58. Kennedy TE, Serafini T, de la Torre JR, Tessier-Lavigne M: Netrins are diffusible chemotropic factors for commissural axons in the embryonic spinal cord. Cell 1994, 78:425–435
59. Stoeckli ET, Landmesser LT: Axonin-1, Nr-CAM, and Ng-CAM play different roles in the in vivo guidance of chick commissural neurons. Neuron 1995, 14:1165–1179
60. Greer JJ, Allan DW, Martin-Caraballo M, Lemke RP: An overview of phrenic nerve and diaphragm muscle development in the perinatal rat. J Appl Physiol 1999, 86:779–786
61. Ptak K, Hilaire G: Central respiratory effects of substance P in neonatal mice: an in vitro study. Neurosci Lett 1999, 266:189–192
62. Greer JJ, Al-Zubaidy ZA, Carter JE: Thyrotropin releasing hormone (TRH) stimulates perinatal rat respiration in vitro. Am J Physiol 1996, 40:R1160–R1164
63. Feldman JL, Mitchell GS, Nattie EE: Breathing: rhythmicity, plasticity, chemosensitivity. Ann Rev Neurosci 2003, 26:239–266
64. Rekling JC, Feldman JL: PreBotzinger complex and pacemaker neurons: hypothesized site and kernel for respiratory rhythm generation. Annu Rev Physiol 1998, 60:385–405
65. Smith JC, Butera RJ, Koshiya N, Del Negro C, Wilson CG, Johnson SM: Respiratory rhythm generation in neonatal and adult mammals: the hybrid pacemaker-network model. Respir Physiol 2000, 122:131–147
66. Greer JJ, Smith JC, Feldman JL: Role of excitatory amino acids in the generation and transmission of respiratory drive in neonatal rat. J Physiol 1991, 437:727–749
67. Funk GD, Smith JC, Feldman JL: Generation and transmission of respiratory oscillations in medullary slices: role of excitatory amino acids. J Neurophysiol 1993, 70:1497–1515
68. Ballanyi K, Onimaru H, Homma I: Respiratory network function in the isolated brainstem-spinal cord of newborn rats. Prog Neurobiol 1999, 59:583–634
69. Lagercrantz H: Neuromodulators and respiratory control during development. Trends Neurosci 1987, 10:368–372
70. Moss IR, Inman JG: Neurochemicals and respiratory control during development. J Appl Physiol 1989, 67:1–13
71. Ohara S, Ukita Y, Ninomiya H, Ohno K: Axonal dystrophy of dorsal root ganglion sensory neurons in a mouse model of Niemann-Pick disease type C. Exp Neurol 2004, 187:289–298
72. Mukoyama M, Yamazaki K, Kikuchi T, Tomita T: Neuropathology of gracile axonal dystrophy (GAD) mouse. An animal model of central distal axonopathy in primary sensory neurons. Acta Neuropathol (Berl) 1989, 79:294–299
73. Wen CY, Tan CK, Wong WC: Experimental degeneration of primary afferent terminals in the cuneate nucleus of the monkey (Macaca fascicularis). J Anat 1979, 128:709–720
74. Fujisawa K, Shiraki H: Study of axonal dystrophy. I. Pathology of the neuropil of the gracile and the cuneate nuclei in ageing and old rats: a stereological study. Neuropathol Appl Neurobiol 1978, 4:1–20
75. Gindhart JG, Chen J, Faulkner M, Gandhi R, Doerner K, Wisniewski T, Nandlestadt A: The kinesin-associated protein UNC-76 is required for axonal transport in the Drosophila nervous system. Mol Biol Cell 2003, 14:3356–3365
76. Gho M, McDonald K, Ganetzky B, Saxton WM: Effects of kinesin mutations on neuronal functions. Science 1992, 258:313–316
77. Johnson JE, Mehler WR, Miquel J: A fine structural study of degenerative changes in the dorsal column nuclei of aging mice. Lack of protection by vitamin E. J Gerontol 1975, 30:395–411
78. Ong WY, Kumar U, Switzer RC, Sidhu A, Suresh G, Hu CY, Patel SC: Neurodegeneration in Niemann-Pick type C disease mice. Exp Brain Res 2001, 141:218–231
79. Cruz JC, Chang TY: Fate of endogenously synthesized cholesterol in Niemann-Pick type C1 cells. J Biol Chem 2000, 275:41309–41316
80. Saigoh K, Wang YL, Suh JG, Yamanishi T, Sakai Y, Kiyosawa H, Harada T, Ichihara N, Wakana S, Kikuchi T, Wada K: Intragenic deletion in the gene encoding ubiquitin carboxy-terminal hydrolase in gad mice. Nat Genet 1999, 23:10–11
81. Ichihara N, Wu J, Chui DH, Yamazaki K, Wakabayashi T, Kikuchi T: Axonal degeneration promotes abnormal accumulation of amyloid beta-protein in ascending gracile tract of gracile axonal dystrophy (GAD) mouse. Brain Res 1995, 695:173–178
82. Kozlov SV, Gerard M, Stewart CL: Morphological analysis of the respiratory pathway in perinatal mice deficient for necdin: a component of the pathology of Prade-Willi syndrome. Soc Neurosci Abs 2001, 694:10
83. Yoshikawa K: Cell cycle regulators in neural stem cells and postmitotic neurons. Neurosci Res 2000, 37:1–14
84. Taniura H, Yoshikawa K: Necdin interacts with the ribonucleoprotein hnRNP U in the nuclear matrix. J Cell Biochem 2002, 84:545–555
85. Takazaki R, Nishimura I, Yoshikawa K: Necdin is required for terminal differentiation and survival of primary dorsal root ganglion neurons. Exp Cell Res 2002, 277:220–232
86. Kuwako K, Taniura H, Yoshikawa K: Necdin-related MAGE proteins differentially interact with the E2F1 transcription factor and the p75 neurotrophin receptor. J Biol Chem 2004, 279:1703–1712
87. Wevrick R, Walker CL, Karten B, Kuny SL, Poulin AA, Lee S: The Prader-Willi syndrome protein necdin interacts with fasciculation and elongation proteins and is essential for axonal outgrowth in the developing mouse brain. Program No. 834.19. 2004 Abstract Viewer/Itinerary Planner. Washington, DC: Society for Neuroscience. Online
88. Swaab DF: Prader-Willi syndrome and the hypothalamus. Acta Paediatr 1997, 423:50–54
89. L'Hermine AC, Aboura A, Brisset S, Cuisset L, Castaigne V, Labrune P, Frydman R, Tachdjian G: Fetal phenotype of Prader-Willi syndrome due to maternal disomy for chromosome 15. Prenat Diagn 2003, 23:938–943
90. Yoshii A, Krishnamoorthy KS, Grant PE: Abnormal cortical development shown by 3D MRI in Prader-Willi syndrome. Neurology 2002, 59:644–645
91. Hayashi M, Itoh M, Kabasawa Y, Hayashi H, Satoh J, Morimatsu Y: A neuropathological study of a case of the Prader-Willi syndrome with an interstitial deletion of the proximal long arm of chromosome 15. Brain Dev 1992, 14:58–62